nagra.

Arbeitsbericht NAB 10-21

Ancillary rock and pore water studies on drillcores from northern Switzerland

August 2011

D. Meier, M. Mazurek

Rock-Water Interaction
Institute of Geological Sciences
University of Bern

**Nationale Genossenschaft
für die Lagerung
radioaktiver Abfälle**

Hardstrasse 73
CH-5430 Wettingen
Telefon 056-437 11 11

www.nagra.ch

nagra.

Arbeitsbericht NAB 10-21

Ancillary rock and pore water studies on drillcores from northern Switzerland

August 2011

D. Meier, M. Mazurek

Rock-Water Interaction
Institute of Geological Sciences
University of Bern

KEYWORDS
Tracer profiles, Chloride, Mineralogy, Porosity, Chlorid, Mineralogie, Porosität, Benken, Riniken, Schafisheim, Weiach, Opalinuston, Effinger Schichten, Brauner Dogger

**Nationale Genossenschaft
für die Lagerung
radioaktiver Abfälle**

Hardstrasse 73
CH-5430 Wettingen
Telefon 056-437 11 11

www.nagra.ch

Nagra Working Reports concern work in progress that may have had limited review. They are intended to provide rapid dissemination of information. The viewpoints presented and conclusions reached are those of the author(s) and do not necessarily represent those of Nagra.

Table of contents

List of Tables

List of Figures

1 Introduction

A laterally extended, about 300 - 600 m thick low-permeability sequence mainly dominated by clay-rich lithologies occurs between the Malm and Triassic (Keuper or Muschelkalk) aquifers of northern Switzerland (an example is provided in Fig. 1). It includes, among other units, three formations that have been proposed by Nagra (2008) as host rocks for various types of radioactive wastes. The five potential siting regions in northern Switzerland and the corresponding host rocks (Opalinus Clay, the overlying "Brauner Dogger"[1] and the Effinger Schichten) are shown in Fig. 2.

This report revisits existing drillcore materials from older boreholes in the region of interest and documents the results of a new analytical campaign. The objectives were to study the spatial distribution of natural-tracer concentrations in pore water at locations where this has not been done previously and to augment the mineralogical data base with respect to the newly proposed host rocks "Brauner Dogger" and Effinger Schichten. The present report has the focus on the tracer profiles. The mineralogical data of the host-rock sections are analysed in Mazurek (2011).

One of the motivations for this report was the success of the campaign for the Benken borehole, where regular profiles of Cl^-, $\delta^{18}O$ and δ^2H were identified across the whole low-permeability sequence (Gimmi & Waber 2004, Gimmi *et al.* 2007). In that campaign, the tracer profiles, together with the known tracer concentrations in the bounding aquifers and palaeo-hydrogeological constraints, were subjected to transport modelling, in order to reproduce the observed profiles using plausible transport parameters and evolution scenarios. That study, together with a suite of studies related to other European sites (Mazurek *et al.* 2009, 2011), provided valuable information pertaining to transport mechanisms and parameters and thereby yielded constraints with regard to the long-term evolution of low-permeability sequences.

In this study, core materials from the low-permeability sequence illustrated in Fig. 1 have been sampled in the boreholes of Weiach (WEI; Matter *et al.* 1988a, Nagra 1989), Riniken (RIN; Matter *et al.* 1987, Nagra 1990) and Schafisheim (SHA; Matter *et al.* 1988b, Nagra 1992), together with additional materials from the Benken borehole (BEN; Nagra 2001). Given the fact that the original pore water is no longer present in these core materials, the spectrum of tracers that could be studied was limited to Cl^- and Br^-. These precipitated as salts when the pore water evaporated but are still present in the rock, unaffected by the environmental conditions during core storage (air humidity, oxidising regime).

[1] Definition according to Nagra (2008): The informal term "Brauner Dogger“ relates to the suite of generally clay-rich rock units stratigraphically located between the Opalinus Clay and the Malm. In the Geological Atlas of Switzerland, these units are shown in brown colours and occur in the Tabular Jura east of the Aare river and the region Zürich-Nordost-Schaffhausen.

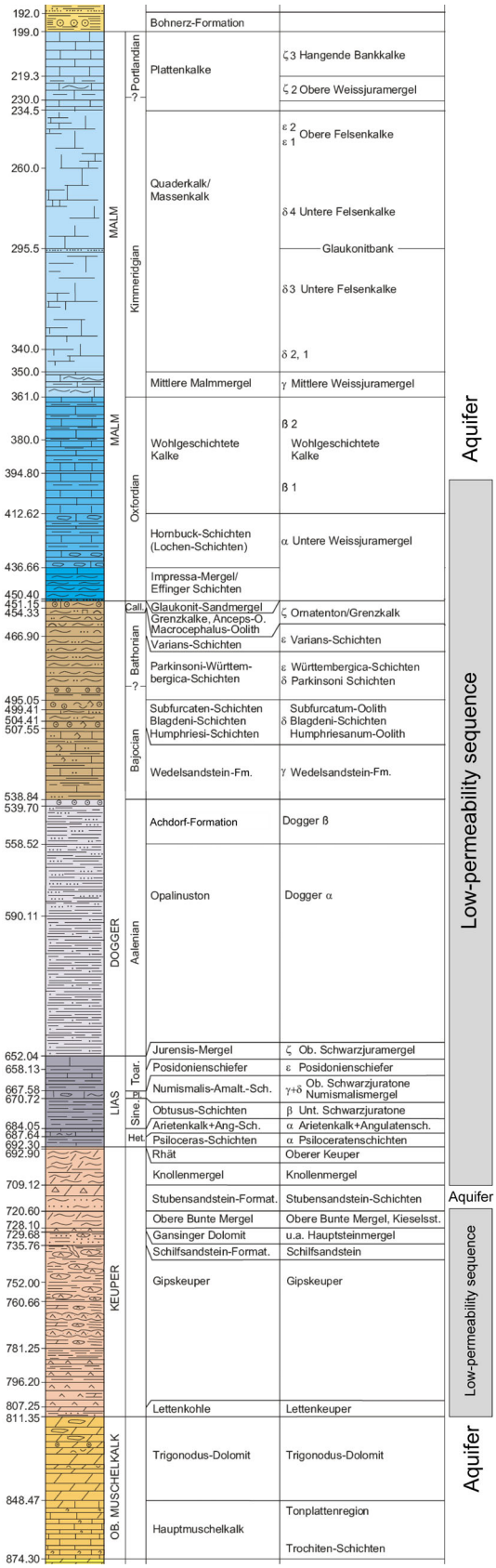

Fig. 1: Geological profile of the Benken borehole, including the distinction of aquifers and low-permeability sequences in the Jurassic and Triassic (adapted from Nagra 2001)

The exact position of the aquifer horizons varies over the region of interest

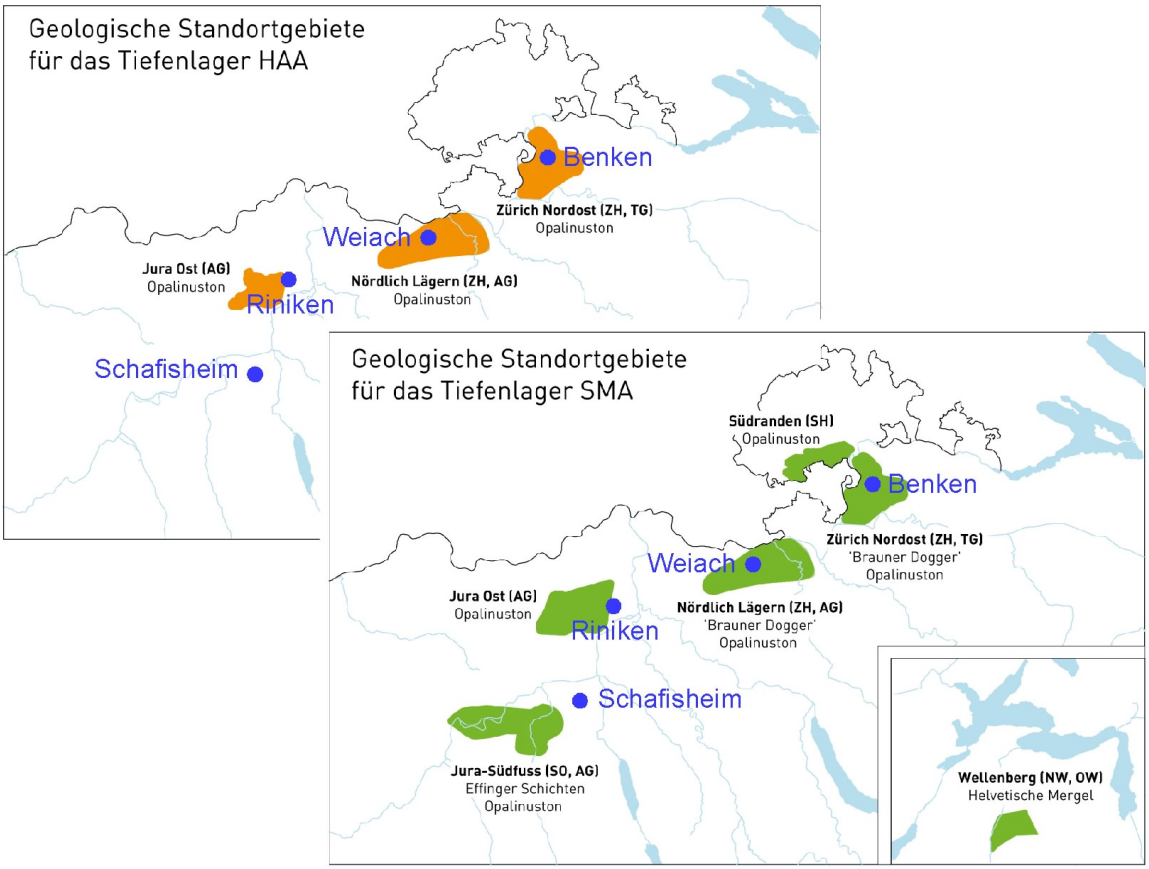

Fig. 2: Potential siting areas and host rocks for geological disposal of high-level (HAA) and low- and intermediate-level (SMA) radioactive waste in Switzerland (adapted from Nagra 2008[2]). Locations of boreholes studied here are shown in blue

[2] The nomenclature of the potential siting areas has recently been updated: Zürcher Weinland → **Zürich Nordost,** Nördlich Lägeren → **Nördlich Lägern,** Bözberg → **Jura Ost.**

2 Sampling

2.1 System geometry

The sequences in Benken and Weiach are bounded by the overlying Malm aquifer constituted of massive limestones. In Riniken, these limestones are missing due to erosion, and the base of the Quaternary is considered as the upper boundary. In Schafisheim, a water sample was taken in the Lower Fresh-Water Molasse in the interval 553 - 563 m. In the footwall of this test, no hydraulic data are available down to the top of the Sowerbyi-Sauzei-Schichten, so the upper boundary cannot be clearly defined. The likely spectrum for its position extends from the base of the Molasse interval from which water was produced (563 m) to the base of the Hauptrogenstein (917 m).

The lower boundary in Benken is constituted of Keuper sandstones. In Riniken, these strata are also taken as the lower boundary, in spite of the lower hydraulic conductivity of 5E-9 m/s in this borehole. In Weiach and Schafisheim, the Keuper has very low hydraulic conductivities. Therefore, the underlying Muschelkalk aquifer is thought to constitute the lower boundary at these sites.

The way the boundaries were defined on the basis of geological information, packer-test results and fluid logs is documented in Tab. 1. In Tab. 2 - 5, the results of pertinent hydraulic tests are summarised, together with information on the chemical composition of ground-water samples taken from the aquifers that embed the low-permeability sequence.

Tab. 1: Definition of the top and bottom boundaries of the low-permeability sequences in boreholes Benken, Riniken, Schafisheim and Weiach

Upper boundary of low-permeability sequence [m]		Lower boundary of low-permeability sequence [m]		Remarks	Missing core section in low-permeability sequence [m]
Benken (BEN)					
397	Basis of major subvertical fracture im Malm limestone from which a water sample was pumped (test M2: 380.0 - 394.8 m)	709.1	Top of porous and brecciated sandstone from which a water sample was pumped in the Keuper (test K2: 698.0 - 739.2 m)		-
Riniken (RIN)					
25.1	Base Quaternary (overlying Effinger Schichten). No packer tests down to 217 m, but no discontinuities in fluid logs at shallow level (Nagra 1988, Beilage 6.1)	513	Packer test 501 - 530.5 m; no discontinuities in fluid logs (Nagra 1988, Beilage 6.1). Depth of 513 m corresponds to the top of the uppermost sandstone within the Schilfsandstein-Formation	Core section within the low-permeability sequence is incomplete	33 - 325.4, 490.2 - 513
Schafisheim (SHA)					
563 - 917	Base of packer test in USM (Lower Freshwater Molasse) to base of Hauptrogenstein (exact position unknown due to absence of hydraulic data)	1227	Discontinuities in fluid logs at 1227, 1236 m (top Muschelkalk; see Nagra 1988, Beilage 7.2)	Keuper "aquifer" has low permeability, the low-permeability sequence reaches down to the Muschelkalk. Core section within the low-permeability sequence is incomplete	563 - 577, 594.8 - 964
Weiach (WEI)					
267	No discontinuities in fluid logs; boundary taken as the base of the packer test in the Malm	822	Packer test 822 - 896.1 m (Muschelkalk); discontinuitues in fluid logs at 822 m (el. conductivity) and 827 m (temperature) (Nagra 1988, Beilage 5.2)	Keuper "aquifer" has low permeability, the low-permeability sequence reaches down to the Muschelkalk	-

Tab. 2: Hydrogeological and hydrochemical information for borehole Benken: Documentation of packer-test intervals, hydraulic conductivities and ground-water compositions in aquifers (from Nagra 2001). The low-permeability sequence is shown in grey, directly embedding aquifers in blue. Further tests and water samples shown in white

Top interval [m]	*Base interval [m]*	*Epoch*	*Formation*	*Quality of water sample*	*Na^+ [mg/L]*	*K^+ [mg/L]*	*Mg^{++} [mg/L]*	*Ca^{++} [mg/L]*	*Cl^- [mg/L]*	*Br^- [mg/L]*	*SO_4^{--} [mg/L]*	*K [m/s]*	*No core [m]*
205.3	394.8											1.1E-08	
380.0	394.8	Malm	Wohlgeschichtete Kalke	usable	3137	53	130	250	4356	6.9	1429	6.7E-10	
403.3	454.6	Malm - Dogger	Wohlgeschichtete Kalke, Hornbuck-Schichten, Effinger Schichten, Glaukonit-Sandmergel, "Brauner Dogger"									5.8E-14	
446.3	497.6	Dogger	Effinger Schichten, Glaukonit-Sandmergel, "Brauner Dogger"									1.6E-13	
496.3	547.6	Dogger	"Brauner Dogger", Achdorf-Formation									2.1E-12	
566.5	596.5	Dogger	Opalinuston									1.3E-14	
600.1	603.5	Dogger	Opalinuston									1.2E-14	
605.1	623.6	Dogger	Opalinuston									5.8E-14	
623.7	655.7	Dogger - Lias	Opalinuston, Jurensis-Mergel									3.7E-14	
656.8	698.0	Lias - Keuper	Lias, Rhät, Knollenmergel									3.0E-14	
698.0	739.2	Keuper	Knollenmergel, Stubensandstein, Obere Bunte Mergel, Gansinger Dolomit, Schilfsandstein, Gipskeuper	good	2800	33	68	210	520	1.0	5900	9.7E-08	
769.7	787.6	Keuper	Gipskeuper									8.4E-14	
813.0	826.0	Muschelkalk	Trigonodus-Dolomit	good	59	11	120	448	75	b.d.	1300	4.6E-07	
813.0	877.2	Muschelkalk	Trigonodus-Dolomit, Hauptmuschelkalk, Dolomit der Anhydritgr.									9.3E-08	
974.3	983.0	(Muschelkalk), Buntsandstein	(Wellendolomit,) Buntsandstein	good	408	7	2	13	252	0.3	210	5.7E-06	

Tab. 3: Hydrogeological and hydrochemical information for borehole Riniken: Documentation of packer-test intervals, hydraulic conductivities and ground-water compositions in aquifers (from Nagra 1990). The low-permeability sequence is shown in grey, directly embedding aquifers in blue. Further tests and water samples shown in white

Top interval [m]	*Base interval [m]*	*Epoch*	*Formation*	*Quality of water sample*	*Na^+ [mg/L]*	*K^+ [mg/L]*	*Mg^{++} [mg/L]*	*Ca^{++} [mg/L]*	*Cl^- [mg/L]*	*Br^- [mg/L]*	*SO_4^{--} [mg/L]*	*K [m/s]*	*No core [m]*
0.0	25.1	Quaternary	Quaternary										
25.1	209.5	Malm	Effinger Schichten Birmenstorfer Sch. Varians-Schichten, Spatkalk, Obere Parkinsoni-Sch.										
217.1	250.9	Dogger										≤1E-12	33 - 325.4
313.4	337.3	Dogger	Sowerbyi-Sauzei-Schichten, Murchisonae-Concava-Schichten, Opalinuston									5.0E-14	
338.7	397.7	Dogger	Opalinuston									2.0E-14	
397.7	430.1	Dogger	Opalinuston									4.0E-14	
433.4	490.2	Dogger/Lias	Opalinuston, Lias, Knollenmergel									6.0E-13	
501.0	530.5	Keuper	Ob. Bunte Mergel, Gansinger Dolomit, Schilfsandstein, Gipskeuper	good	4263	54	203	585	2775	6.6	7314	5.0E-09	490.2 - 624.5, 629.5 - 696.0
617.3	696.0	Muschelkalk	Trigonodus-Dolomit, Hauptmuschelkalk, Dolomit der Anhydritgruppe	good	3998	46	210	874	6008	0.7	3011	7.0E-07	
701.5	748.5	Muschelkalk	Obere Sulfatschichten, Salzschichten, Untere Sulfatschichten									≤1E-12	
													757.5 - 793.9
793.0	820.2	Buntsandstein	Buntsandstein, (Rotliegendes)	good	2949	102	61	496	4030	10.2	1850	1.5E-06	

Tab. 4: Hydrogeological and hydrochemical information for borehole Schafisheim: Documentation of packer-test intervals, hydraulic conductivities and ground-water compositions in aquifers (from Nagra 1992). The low-permeability sequence is shown in grey, directly embedding aquifers in blue. Further tests and water samples shown in white

Top interval [m]	*Base interval [m]*	*Epoch*	*Formation*	*Quality of water sample*	*Na^+ [mg/L]*	*K^+ [mg/L]*	*Mg^{++} [mg/L]*	*Ca^{++} [mg/L]*	*Cl^- [mg/L]*	*Br^- [mg/L]*	*SO_4^{--} [mg/L]*	*K [m/s]*	*No core [m]*
													-290
553.0	563.0	Tertiary	USM	very good	3032	19	68	209	5208	20.3	5	5.0E-08	314.9 - 577
961.4	987.7	Dogger	Sowerbyi-Sauzei-Schichten									≤1.0E-14	594.8 - 964
989.3	1017.2	Dogger	Sowerbyi-Sauzei-Sch., Murchisonae-Concava-Schichten, Opalinuston									≤5.0E-13	
1001.3	1029.2	Dogger	Opalinuston									≤5.0E-13	
1028.9	1056.7	Dogger	Opalinuston									≤2.0E-13	
1051.7	1079.6	Dogger	Opalinuston									≤5.0E-13	
1080.5	1108.4	Lias	Lias, Knollenmergel									≤3.0E-13	
1112.2	1140.1	Keuper	Gansinger Dolomit, Schilfsandstein									≤1.0E-11	
1238.6	1259.5	Muschelkalk	Trigonodus-Dolomit, Hauptmuschelkalk									5.0E-08	1235 - 1252, 1257.3 - 1260.9
1227.8	1293.0	Muschelkalk	Hauptmuschelkalk, Dolomit der Anhydritgr.	very good	4490	113	174	743	6400	6.6	2805	1.0E-07	
1240.7	1261.6	Muschelkalk	Trigonodus-Dolomit, Hauptmuschelkalk	usable	4700	115	184	784	6700	5.6	2850		1274.8 - 1285.0
1318.5	1356.9	Muschelkalk	Obere Sulfatschichten, Dolomit der Anhydritgr. (Aufschiebungszone), Hauptmuschelkalk, Dolomit der Anhydritgr.									≤5.0E-12	1338 - 1349.3
1356.2	1398.3	Muschelkalk	Obere Sulfatschichten, Salzschichten, "Mittlere" Sulfatschichten									<1.0E-16	
1396.3	1438.4	Muschelkalk	"Mittlere" Sulfatschichten, Salzschichten, Untere Sulfatschichten									<1.0E-16	
1476.0	1500.4	Muschelkalk / Buntsandstein / Basement	Wellendolomit, Buntsandstein, Basement	usable - good	4955	132	67	532	6405	11.6	3083	6.0E-10	1448.2 - 1481.8

Tab. 5: Hydrogeological and hydrochemical information for borehole Weiach: Documentation of packer-test intervals, hydraulic conductivities and ground-water compositions in aquifers (from Nagra 1989). The low-permeability sequence is shown in grey, directly embedding aquifers in blue. Further tests and water samples shown in white

Top interval [m]	Base interval [m]	Epoch	Formation	Quality of water sample	Na^+ [mg/L]	K^+ [mg/L]	Mg^{++} [mg/L]	Ca^{++} [mg/L]	Cl^- [mg/L]	Br^- [mg/L]	SO_4^{--} [mg/L]	K [m/s]	No core [m]
188.0	202.0	Malm	Massenkalk	not usable								6.0E-08	
242.9	267.0	Malm	Massenkalk	usable	2275	29	91	148	3797	11.5	33	3.0E-07	
472.0	487.2	Dogger/Malm	Effinger Sch., Birmenstorfer Sch., Glaukonit-Sandmergel, "Brauner Dogger"									very low permeability	
543.0	557.0	Dogger	"Brauner Dogger", Opalinuston									3.0E-13	
692.0	706.0	Lias/Keuper	Lias, Knollenmergel									not quantifiable	
715.9	740.0	Keuper	Knollenmergel, Stubensandstein, Ob. Bunte Mergel, Gansinger Dolomit, Schilfsandstein									6.0E-11	
822.0	896.1	Muschelkalk	Trigonodus-Dolomit, Hauptmuschelkalk, Dolomit der Anhydritgr.	usable	139	25	149	579	53	b.d.	1990	1.0E-6, 1.0E-7	
901.4	950.9	Muschelkalk	Sulfatschichten, Orbicularis-Mergel, Wellenmergel									3.0E-13	
983.0	985.3	Buntsandstein	Buntsandstein	not usable									
981.0	989.6	Buntsandstein	Buntsandstein	good	4318	81	65	457	2921	6.9	6198	2.0E-07	

2.2 Sampling strategy

Over the entire low-permeability sequences in boreholes Benken, Riniken, Schafisheim and Weiach, the objective was to take a sample approximately every 10 m along hole. In practice, there were the following deviations from this principle:

- In boreholes Riniken and Schafisheim, core materials are not available from parts of the depth intervals of interest (Tab. 3 - 4, Fig. 3). The biggest gaps are in the upper part of the low-permeability sequence.
- Borehole Benken has been studied in detail previously (Nagra 2001, Gimmi & Waber 2004, Gimmi *et al.* 2007). Sampling for this study was limited to the "Brauner Dogger" (in order to increase the data base from this somewhat heterogeneous sequence) and to the lowermost part of the Malm (from which no samples had been taken previously).
- In the Weiach core, a set of 19 samples between the upper Keuper and the "Brauner Dogger" has been studied by H. N. Waber in 2000 (mineralogy, anion contents based on aqueous extracts; undocumented work). These data were integrated into the present work without re-sampling this interval, with the exception of 3 new samples that were taken to obtain an even denser coverage of the profile.

Finally, a total of 94 samples were collected for this study.

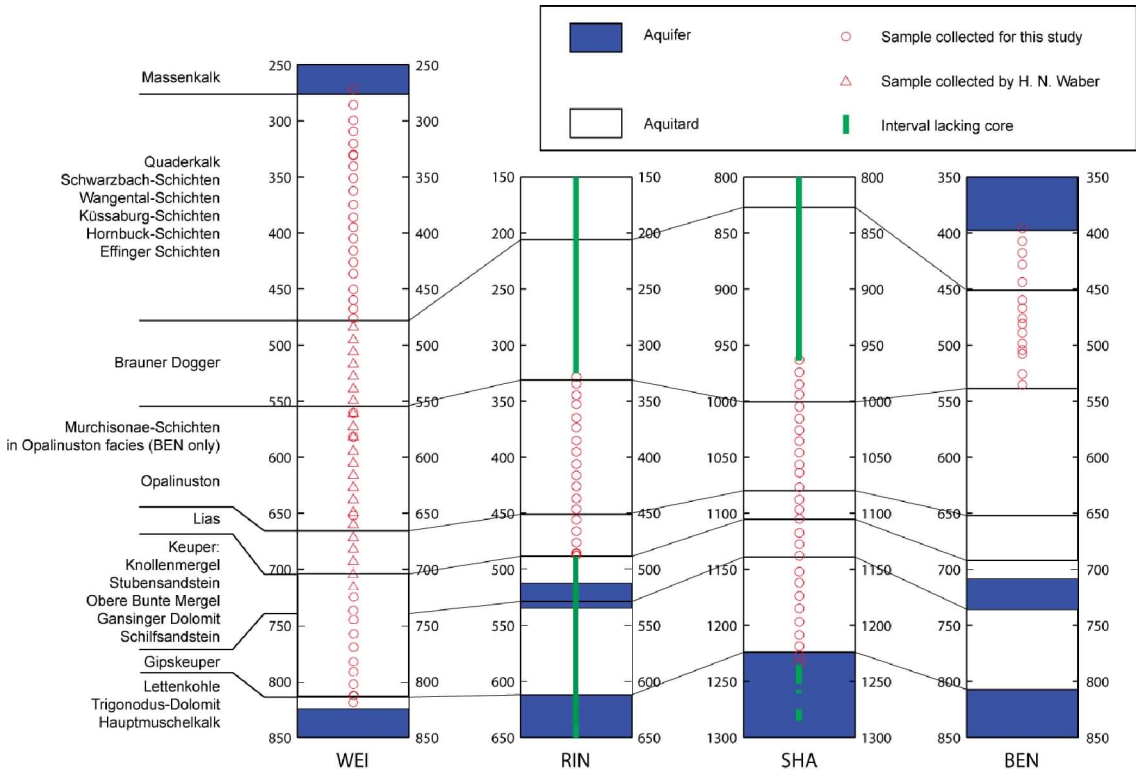

Fig. 3: Schematic sections of boreholes Benken, Riniken, Schafisheim and Weiach, showing the hydrogeological properties and the sampling positions

2.3 Sample selection

Samples of about 20 cm length were selected within approximately 3 metres around the predefined depth (corresponding to a sample interval of 10 m) according to the following criteria (with decreasing priority):

- Lithological homogeneity (including absence of veins and joints)
- High clay-mineral content
- Sample integrity

Samples with high clay-mineral contents were often fragmented into several pieces (Fig. 4). Nevertheless, they were preferred for sampling over the more intact calcareous rocks because of their higher expected porosity and original water content. Therefore, the samples are not necessarily representative for a certain interval in terms of lithology, mineralogy, porosity and density, and there may be a slight bias towards clay-rich rocks. The issue of representativity is evaluated in more detail in Mazurek (2011). In terms of pore-water composition, the sampling strategy does not result in any bias because 1) the same solid phases occur in calcareous and shaly beds (even though in different proportions), and 2) diffusion in the connected pore space efficiently levels out local chemical heterogeneities.

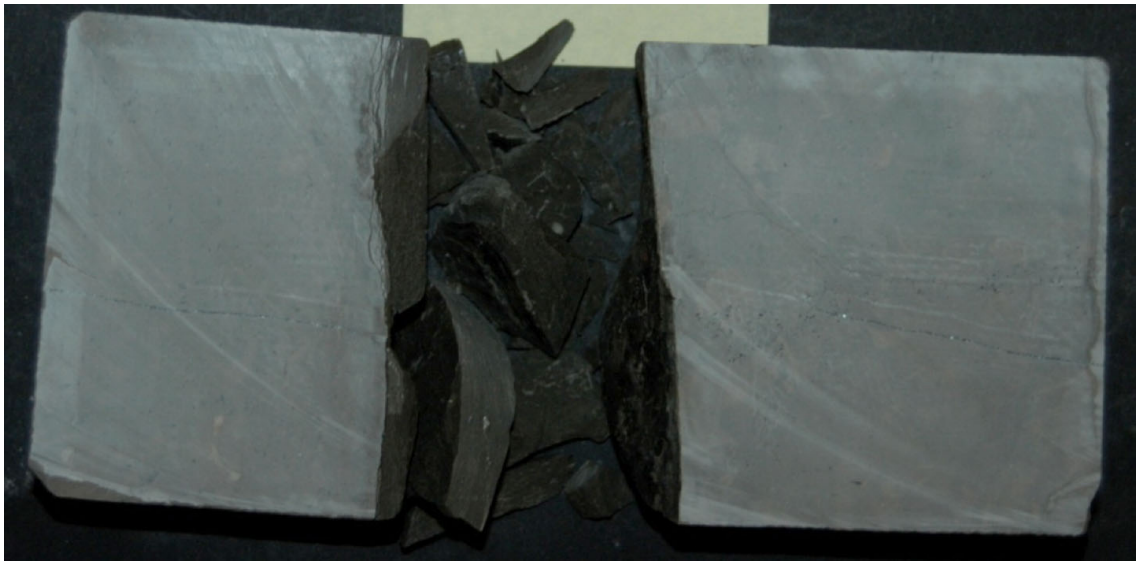

Fig. 4: Sample BEN 407.38, consisting of a layer of argillaceous material within limestone beds. Width of photograph is 20 cm

3 Methods

3.1 Sample preparation

Samples were treated dry, and no cutting with a water-cooled diamond blade was involved. In cases when a sample was macroscopically homogeneous and there was plenty of material, only a part of the sample was crushed. In heterogeneous samples such as that shown in Fig. 4, only one type of material was selected. If possible, the more clay-rich part was selected, but in the majority of the cases there was not enough clay-rich material, and so the more calcareous part of the sample was processed.

After the separation of at least two representative subsamples for bulk dry density measurements, the 1 - 2 kg of sample material were crushed manually with hammer and chisel to pieces of about 1 cm size and then passed through a splitter. A split of about 300 g was ground in a tungsten carbide cup mill (100 g for about 30 s, resulting in a maximum grain size around 1 mm, and 200 g for about 2 min, yielding powders <63 μm).

3.2 Densities / Porosity

3.2.1 Bulk dry density

The bulk dry density $\rho_{b,dry}$ was measured using the paraffin displacement method. The principle of the method is the calculation of bulk dry density from sample mass and volume making use of Archimedes' principle. Two separate and representative rock pieces with a volume of approximately 2-3 cm^3 each were dried at 105 °C. The sample volume was determined by weighing the rock sample in air and during immersion into paraffin oil ($\rho_{paraffin}$ = 0.86 g/cm^3 at 20 °C) using a density accessory kit (Mettler Toledo). The bulk dry density was calculated according to:

$$\rho_{b,dry} = \rho_{paraffin} \frac{m_{dry}}{m_{dry} - m_{in\ paraffin}} \quad .$$

In data tables, the small-scale lithological heterogeneity is represented by the standard deviation of measurements on different subsamples. The analytical error of each individual measurement is dominated by the error on the density of the paraffin (0.86 ±0.01 g/cm^3), which corresponds to an error on $\rho_{b,dry}$ of ±1.2 %. Further sources of uncertainty include the representativity of the small rock pieces for the whole sample, the effects of drying (possible shrinkage of clay-rich samples) and of long-term storage (textural changes due to recurrent changes of temperature and air humidity, oxidation reactions; see Section 5.2 and Section 5.4).

3.2.2 Grain density

The grain density ρ_g was measured by kerosene pycnometry in duplicate. The volume of the pycnometer was derived from the weight of kerosene that filled the pycnometer without rock powder. The density of kerosene (ρ_k = 0.78 g/cm^3 at 20 °C) was checked using an aerometer. After drying the powdered samples at 105 °C, approximately 15 g were placed in the pycnometer. The empty (m_{pycn}) and the filled ($m_{rock+pycn}$) flasks were weighed. The flask was subsequently filled with kerosene up to the meniscus while continuously removing the air by a vacuum pump and then weighed again ($m_{rock+k+pycn}$). The grain density was obtained according to

$$\rho_g = \rho_{kerosene} \frac{m_{rock+pycn} - m_{pycn}}{m_{rock+pycn} - m_{pycn} + m_{k+pycn} - m_{rock+k+pycn}}$$

Some uncertainty mainly roots in the filling of the flask up to the meniscus. Care has to be taken when evacuating the flasks, in order to remove all air from the slurry (remaining air would lead to an underestimation of grain density). As for bulk dry density, the lithological heterogeneity on the sample scale is stated in data tables, represented by the standard deviation of measurements on different subsamples. The analytical uncertainty of each measurement is dominated by the error on the kerosene density (0.78 ±0.01 g/cm^3) and yields an error for ρ_g of ±1.3 %.

3.2.3 Physical porosity

The physical porosity n is calculated from the bulk dry density and the grain density according to

$$n = 1 - \frac{\rho_{b,dry}}{\rho_g}$$

For the uncertainty calculation, the Gaussian law of uncertainty propagation was applied. Let y be calculated from measured parameters x_1, x_2, ... with corresponding uncertainties u_1, u_2, ... The uncertainty of y (u_y) is then defined by

$$u_y = \sqrt{\sum_{i=1}^{n} \left(\frac{\partial y}{\partial x_i} u_i\right)^2}$$

This means for the uncertainty in the particular case for the physical porosity:

$$u_n = \sqrt{\left(-\frac{u_{\rho_{b,dry}}}{\rho_g}\right)^2 + \left(\frac{\rho_{b,dry}\, u_{\rho_g}}{\rho_g^2}\right)^2}$$

In data tables, only the analytical errors on the density measurements were included in the calculation of the error on porosity, whereas lithological heterogeneity and other uncertainties, such as oxidation effects, were not considered at this stage.

3.3 Mineralogy

3.3.1 Whole-rock mineralogy by X-ray diffraction

For quantitative determination of the mineralogical composition, 3 g of each powdered sample were mixed with lithium fluoride (LiF) as an internal standard with a ratio of 10:1. Disoriented samples were measured on a Philips PW 1800 diffractometer using Cu Kα radiation. One X-ray pattern within the 2Θ range from 4° to 60° and one from 25° to 32° (duplicate) were recorded for each sample. In addition, a data acquisition program (GMP) that sweeps for a particular peak in a limited (±1°) 2Θ range and then measures the peak for 100 seconds was used on both duplicate samples. This, together with a measurement of either one or two background values at fixed 2Θ, allowed a more precise quantification than reading the counts from the regular X-ray pattern.

Calibration curves allowing an automatic quantification exist for quartz, calcite, dolomite, K-feldspar and plagioclase. Siderite was quantified by manually reading the intensity from the X-

ray pattern and assuming the same concentration to intensity ratio as for the predominant carbonate (calcite or dolomite). However, the standardisation used for carbonates is only valid for individual mineral contents up to 50 %, which are exceeded in limestones. Therefore, the total inorganic carbon content determined by CS-Mat IR spectroscopy (see Section 3.3.3) was used to correct the carbonate contents. Pyrite content, which can only be qualitatively measured by XRD, was calculated from the S content obtained from the CS-Mat analysis, assuming that pyrite is the only S-containing phase. In cases where anhydrite was detected by XRD, all S was allocated to this phase, and no entry was made for pyrite.

When both anhydrite and dolomite were present (a common mineral assemblage in the Gipskeuper sequence), both peaks of the internal standard (LiF) interfere with the mineral peaks. To allow a quantitative measurement, another internal standard (such as fluorite; CaF_2) could have been used. However, in this study, a Rietveld refinement method using structural data for LiF, anhydrite and dolomite was applied. This does not yield useful results directly because feldspars and phyllosilicates are difficult to refine due to their complex structure and chemical variability. Instead, the proportion of LiF contributing to the 38.6° peak (which is overlain by anhydrite) was estimated. This proportion has then been used to correct the regular GMP calculations. In cases where there was only little quartz and feldspar (the only minerals not corrected by CS-Mat), a semiquantitative RIR method was applied, as even major uncertainties would have a limited effect.

For every single sample, the X-ray pattern was assessed visually as well, in order to check for additional phases and to verify the results of the automatic calculations. The sum of sheet silicates, mainly clay minerals, was calculated by difference to 100 %.

3.3.2 Clay mineralogy by X-ray diffraction

To quantify the relative proportions of clay minerals, the <2µm fraction of the coarsely ground samples was separated by sedimentation in a 20 cm high Atterberg cylinder filled with a 0.01N NH_4OH solution over 16 hours. The slurry was decarbonated using hydrochloric acid (HCl) and saturated with $CaCl_2$, to replace the exchangeable cations by Ca. After pipetting the suspension on glass slides, one sample was dried under air, one was saturated with ethylene glycol ($C_2H_6O_2$), and the third was heated for one hour at 550 °C. Ethylene glycol is used for the identification of expandable clay minerals, while the heating destroys kaolinite and allows a distinction from chlorite.

The three slides were scanned using a Philips PW 3710 diffractometer. Quantification of illite, chlorite, kaolinite and illite-smectite mixed layers was carried out visually by comparing peak intensities or areas.

3.3.3 CS-Mat IR spectroscopy

A rock powder (20 - 100 mg) was heated to 1350 - 1550 °C in an O_2 or N_2 atmosphere, and all volatile components were liberated at these temperatures. Total C and S were measured as CO_2 and SO_2 after oxidation in an O_2 atmosphere. Inorganic C (*i.e.* essentially CO_2 from carbonate minerals) was measured in a N_2 atmosphere, assuming that the content of organic CO_2 is negligible (this is mostly a reasonable assumption, but exceptions exist, *e.g.* some soils). The reaction gas was passed through a Mg perchlorate tube to remove water and then pumped through the CO_2 and SO_2 analysers. The peaks of CO_2 and SO_2 in the carrier gas were measured by IR spectroscopy. Separate NDIR analysers were used for each of the two species. Organic C was calculated by difference of total and inorganic C. Calibration was performed using pure $CaCO_3$ for C and Ag_2SO_4 for S. Approximate detection limits are around 0.1 wt.-% for total C and S.

3.4 Aqueous extraction

Aqueous extraction tests were performed at a solid:liquid (S:L) mass ratio of 1. The amount of pulped rock material was around 30 g. Each sample was prepared, extracted and analysed in duplicate under ambient conditions. Each suspension was shaken end-over-end for 24 hours in a polypropylene tube. After filtration using 0.45 µm millipore filters, the supernatant solutions were analysed for anions (F^-, Cl^-, SO_4^{--}, NO_3^-) by ion chromatography, using a Metrohm 861 Compact IC-system. Br^- and I^- contents were obtained by ICP-MS at the British Geological Survey (BGS, Keyworth, UK).

4 Results

This section documents the results of the study together with data produced by H. N. Waber in 2000 for a set of samples from Weiach (termed here WEI-1 to WEI-22). Waber's data include mineralogy and anion contents, whereas no densities were obtained and so no direct measure of physical porosity was available. Densities of these samples were measured within the frame of this study on the original sample materials, but the results are not applicable for reasons discussed in Section 4.2. A list of all samples is provided in Tab. 6 - 9.

Tab. 6: Benken: List of samples and lithological classification according to the scheme of Füchtbauer (1988), based on the instrumental mineralogical analyses (see below)

Lab ID	Depth [m]	Formation	Lithology (German)	Lithology (English)
BEN 1	395.97	Wohlgeschichtete Kalke	Kalk	Limestone
BEN 2	407.38	Wohlgeschichtete Kalke	Kalk	Limestone
BEN 3	417.83	Hornbuck-Schichten	Kalk	Limestone
BEN 4	428.11	Hornbuck-Schichten	Kalkmergel	Calcareous marl
BEN 5	443.83	Effinger Schichten	Toniger Kalk	Argillaceous limestone
BEN 6	459.90	Varians-Schichten	Kalkiger Sandtonstein	Calcareous sandy clay-rock
BEN 7	467.12	Parkinsoni-Württemb.-Sch.	Kalkiger sandiger Tonstein	Calcareous sandy clay-rock
BEN 8	476.14	Parkinsoni-Württemb.-Sch.	Sandiger toniger Kalk	Sandy argillaceous limestone
BEN 9	481.11	Parkinsoni-Württemb.-Sch.	Kalkiger sandiger Tonstein	Calcareous sandy clay-rock
BEN 20	482.00	Parkinsoni-Württemb.-Sch.	Sandiger Tonmergel	Sandy argillaceous marl
BEN 10	489.15	Parkinsoni-Württemb.-Sch.	Kalkiger Sandtonstein	Calcareous sandy clay-rock
BEN 11	498.61	Subfurcaten-Schichten	Sandiger Kalkmergel	Sandy calcareous marl
BEN 12	504.45	Subfurcaten-Schichten	Sandiger Kalkmergel	Sandy calcareous marl
BEN 13	507.87	Wedelsandstein-Formation	Kalkiger Sandtonstein	Calcareous sandy clay-rock
BEN 21	525.45	Wedelsandstein-Formation	Toniger Kalksandstein	Calcareous argillaceous sandstone
BEN 14	525.88	Wedelsandstein-Formation	Kalksandstein	Calcareous sandstone
BEN 15	535.49	Wedelsandstein-Formation	Sandmergel	Sandy marl

Tab. 7: Riniken: List of samples and lithological classification according to the scheme of Füchtbauer (1988), based on the instrumental mineralogical analyses (see below)

Lab ID	Depth [m]	Formation	Lithology (German)	Lithology (English)
RIN 1	328.34	Murchisonae-Schichten	Tonsandstein	Argillaceous sandstone
RIN 2	334.68	Opalinuston	Sandmergel	Sandy marl
RIN 3	344.72	Opalinuston	Kalkiger Sandtonstein	Calcareous sandy clay-rock
RIN 4	352.91	Opalinuston	Kalkiger Sandtonstein	Calcareous sandy clay-rock
RIN 5	365.03	Opalinuston	Kalkiger Sandtonstein	Calcareous sandy clay-rock
RIN 6	373.60	Opalinuston	Kalkiger Sandtonstein	Calcareous sandy clay-rock
RIN 7	385.16	Opalinuston	Kalkiger Sandtonstein	Calcareous sandy clay-rock
RIN 8	395.20	Opalinuston	Kalkiger sandiger Tonstein	Calcareous sandy clay-rock
RIN 9	406.03	Opalinuston	Kalkiger Sandtonstein	Calcareous sandy clay-rock
RIN 10	416.28	Opalinuston	Kalkiger Sandtonstein	Calcareous sandy clay-rock
RIN 11	426.03	Opalinuston	Kalkiger sandiger Tonstein	Calcareous sandy clay-rock
RIN 12	436.81	Opalinuston	Kalkiger sandiger Tonstein	Calcareous sandy clay-rock
RIN 13	446.51	Opalinuston	Kalkiger sandiger Tonstein	Calcareous sandy clay-rock
RIN 14	455.84	Posidonienschiefer	Sandiger Tonmergel	Sandy argillaceous marl
RIN 15	466.07	Obtusus-Ton	Kalkiger toniger Sandstein	Calcareous agrillaceous sandstone
RIN 16	476.25	Arietenkalk	Tonsandstein	Argillaceous sandstone
RIN 17	485.67	Insektenmergel	Kalkiger sandiger Tonstein	Calcareous sandy clay-rock
RIN 18	487.70	Insektenmergel	Sandtonstein	Sandy clay-rock

Tab. 8: Schafisheim: List of samples and lithological classification according to the scheme of Füchtbauer (1988), based on the instrumental mineralogical analyses (see below)

Lab ID	Depth [m]	Formation	Lithology (German)	Lithology (English)
SHA 1	963.05	Sowerbyi-Sauzei-Schichten	Sandiger Kalkmergel	Sandy calcareous marl
SHA 2	974.32	Sowerbyi-Sauzei-Schichten	Kalksandstein	Calcareous sandstone
SHA 3	985.03	Sowerbyi-Sauzei-Schichten	Kalkiger Tonsandstein	Calcareous argillaceous sandstone
SHA 4	994.20	Murchisonae-Schichten	Kalksandstein	Calcareous sandstone
SHA 5	1005.10	Opalinuston	Kalkiger Sandtonstein	Calcareous sandy clay-rock
SHA 6	1015.67	Opalinuston	Kalkiger Sandtonstein	Calcareous sandy clay-rock
SHA 7	1026.11	Opalinuston	Kalkiger Sandtonstein	Calcareous sandy clay-rock
SHA 8	1035.75	Opalinuston	Kalkiger Sandtonstein	Calcareous sandy clay-rock
SHA 9	1046.03	Opalinuston	Kalkiger Sandtonstein	Calcareous sandy clay-rock
SHA 10	1056.63	Opalinuston	Kalkiger Sandtonstein	Calcareous sandy clay-rock
SHA 11	1063.95	Opalinuston	Kalkiger sandiger Tonstein	Calcareous sandy clay-rock
SHA 12	1076.86	Opalinuston	Kalkiger Sandtonstein	Calcareous sandy clay-rock
SHA 13	1087.78	Obtusus-Ton	Sandmergel	Sandy marl
SHA 14	1096.88	Insektenmergel	Kalkiger sandiger Tonstein	Calcareous sandy clay-rock
SHA 15	1105.10	Insektenmergel	Dolomitischer sandiger Tonstein	Dolomitic sandy clay-rock
SHA 16	1117.57	Schilfsandstein	Anhydritführender sandiger Tonmergel	Anhydritic sandy argillaceous marl
SHA 17	1127.74	Schilfsandstein	Sandtonstein	Sandy clay-rock
SHA 18	1138.08	Schilfsandstein	Anhydritischer Tonsandstein	Anhydritic argillaceous sandstone
SHA 19	1152.15	Gipskeuper	Anhydritischer Tonmergel	Anhydritic argillaceous sandstone
SHA 20	1162.05	Gipskeuper	Toniger Anhydrit	Argillaceous anhydrite
SHA 21	1173.84	Gipskeuper	Sandiger toniger Anhydrit	Sandy argillaceous anhydrite
SHA 22	1184.98	Gipskeuper	Anhydritischer Tonmergel	Anhydritic argillaceous marl
SHA 23	1196.99	Gipskeuper	Dolomitischer stark toniger Anhydrit	Dolomitic argillaceous anhydrite
SHA 24	1208.68	Gipskeuper	Dolomitischer stark toniger Anhydrit	Dolomitic argillaceous anhydrite
SHA 25	1218.59	Gipskeuper	Anhydrit	Anhydrite
SHA 26	1226.69	Lettenkohle	Anhydritführender Dolomit	Anhydritic dolostone
SHA 27	1234.28	Trigonodus-Dolomit	Anhydritführender Dolomit	Anhydritic dolostone

Tab. 9: Weiach: List of samples and lithological classification according to the scheme of Füchtbauer (1988), based on the instrumental mineralogical analyses (see below)

Lab ID	Depth [m]	Formation	Lithology (German)	Lithology (English)
WEI 31	271.98	Massenkalk	Toniger Kalk	Argillaceous limestone
WEI 32	285.77	Quaderkalk	Toniger Kalk	Argillaceous limestone
WEI 33	299.52	Schwarzbach-Schichten	Toniger Kalk	Argillaceous limestone
WEI 34	309.33	Schwarzbach-Schichten	Kalkmergel	Calcareous marl
WEI 35	320.25	Wangental-Schichten	Toniger Kalk	Argillaceous limestone
WEI 36	330.06	Wangental-Schichten	Kalk	Limestone
WEI 37	330.88	Wangental-Schichten	Kalk	Limestone
WEI 25	340.51	Küssaburg-Schichten	Toniger Kalk	Argillaceous limestone
WEI 38	351.14	Küssaburg-Schichten	Kalk	Limestone
WEI 39	362.41	Küssaburg-Schichten	Kalk	Limestone
WEI 40	374.73	Küssaburg-Schichten	Toniger Kalk	Argillaceous limestone
WEI 41	386.05	Hornbuck-Schichten	Toniger Kalk	Argillaceous limestone
WEI 42	394.91	Effinger Schichten	Toniger Kalk	Argillaceous limestone
WEI 43	404.98	Effinger Schichten	Sandiger toniger Kalk	Sandy argillaceous limestone
WEI 44	415.79	Effinger Schichten	Toniger Kalk	Argillaceous limestone
WEI 45	426.14	Effinger Schichten	Toniger Kalk	Argillaceous limestone
WEI 46	436.39	Effinger Schichten	Kalkmergel	Calcareous marl
WEI 47	450.30	Effinger Schichten	Kalkmergel	Calcareous marl
WEI 48	459.69	Effinger Schichten	Sandiger toniger Kalk	Sandy argillaceous limestone
WEI 49	467.84	Effinger Schichten	Toniger Kalk	Argillaceous limestone
WEI 50	476.09	Effinger Schichten	Toniger Kalk	Argillaceous limestone
WEI 1	484.14	Varians-Schichten	Kalkiger sandiger Tonstein	Calcareous sandy clay-rock
WEI 2	495.46	Württembergica-Schichten	Sandmergel	Sandy marl
WEI 3	506.08	Württembergica-Schichten	Sandiger Tonmergel	Sandy argillaceous marl
WEI 4	517.10	Württembergica-Schichten	Kalkiger sandiger Tonstein	Calcareous sandy clay-rock
WEI 5	527.86	Parkinsoni-Schichten	Sandmergel	Sandy marl
WEI 6	539.26	Sowerbyi-Sauzei-Schichten	Kalkiger sandiger Tonstein	Calcareous sandy clay-rock
WEI 7	549.62	Murchisonae-Schichten	Sandiger Tonstein	Sandy clay-rock
WEI 51	560.48	Opalinuston	Toniger stark sandiger Kalk	Sandy argillaceous limestone
WEI 8	561.08	Opalinuston	Kalkiger Sandtonstein	Calcareous sandy clay-rock
WEI 9	572.80	Opalinuston	Kalkiger sandiger Tonstein	Calcareous sandy clay-rock
WEI 52	581.86	Opalinuston	Kalkiger Sandtonstein	Calcareous sandy clay-rock
WEI 10	582.04	Opalinuston	Kalkiger Sandtonstein	Calcareous sandy clay-rock
WEI 11	594.74	Opalinuston	Sandtonstein	Sandy clay-rock
WEI 12	605.34	Opalinuston	Kalkiger sandiger Tonstein	Calcareous sandy clay-rock
WEI 13	616.32	Opalinuston	Kalkiger Sandtonstein	Calcareous sandy clay-rock
WEI 14	627.09	Opalinuston	Kalkiger sandiger Tonstein	Calcareous sandy clay-rock
WEI 15	638.09	Opalinuston	Kalkiger sandiger Tonstein	Calcareous sandy clay-rock
WEI 16	649.46	Opalinuston	Kalkiger sandiger Tonstein	Calcareous sandy clay-rock
WEI 53	652.20	Opalinuston	Kalkiger sandiger Tonstein	Calcareous sandy clay-rock
WEI 17	660.30	Opalinuston	Kalkiger sandiger Tonstein	Calcareous sandy clay-rock
WEI 18	671.89	Posidonienschiefer	Kalkmergel	Calcareous marl
WEI 19	682.16	Obtusus-Ton	Kalkiger Tonsandstein	Calcareous argillaceous sandstone
WEI 20	693.19	Obtusus-Ton	Kalkiger Sandtonstein	Calcareous sandy clay-rock
WEI 21	703.88	Insektenmergel	Kalkiger sandiger Tonstein	Calcareous sandy clay-rock
WEI 22	715.56	Knollenmergel	Sandiger Tonmergel	Sandy argillaceous marl
WEI 54	723.98	Obere Bunte Mergel	Sandiger Tonmergel	Sandy argillaceous marl
WEI 55	736.12	Schilfsandstein	Sandiger Tonstein	Sandy clay-rock
WEI 56	744.63	Gipskeuper	Anhydritführender sandiger Tonmergel	Anhydritic sandy argillaceous marl
WEI 57	757.94	Gipskeuper	Anhydritführender Sandmergel	Anhydritic sandy marl
WEI 58	769.10	Gipskeuper	Dolomitischer toniger Anhydrit	Dolomitic argillaceous anhydrite
WEI 59	782.38	Gipskeuper	Toniger dolomitischer Anhydrit	Argillaceous dolomitic anhydrite
WEI 60	790.71	Gipskeuper	Anhydritf. dolom. sandiger Tonstein	Anhydritic dolomitic sandy clay-rock
WEI 61	802.29	Gipskeuper	Anhydritischer Tonmergel	Anhydritic argillaceous marl
WEI 62	812.25	Gipskeuper	Stark dolomitischer Anhydrit	Dolomitic anhydrite
WEI 63	818.50	Lettenkohle	Sandtonstein	Sandy clay-rock

4.1 Mineralogical composition

The whole-rock mineralogical compositions, including the CS-Mat measurements, are given in Tab. 10 - 13. The investigated rocks span a wide range of compositions, from clay-rocks over limestones to evaporites. The resulting lithological classification of the samples after Füchtbauer (1988) is shown in Tab. 6 - 9. Both German and English names are given because the German classification makes more subdivisions (Example: A carbonate-free rock is called "sandy clay-rock" for clay-mineral contents from 50 to 90 %. In German, the terms "Sandtonstein" or "Sandiger Tonstein" are used, with a threshold clay-mineral content of 75 %).

Fig. 5 shows the rock compositions in a ternary plot. Evaporites containing >10 % anhydrite are not shown in this Figure. It can be seen that the Malm sequence lies in the carbonate-rich part of the diagram and shows quartz contents that rarely exceed 10 %. The Opalinus Clay, on the other hand, lies almost entirely in the field of sandy calcareous clay-rock. The "Brauner Dogger", Lias and Keuper sequences are more scattered, although at Benken, parts of the "Brauner Dogger" sequence are within the compositional range for Opalinus Clay. This is the case for some samples of the Lias and Keuper sequences from all studied boreholes as well.

Clay mineralogy was only studied for selected samples from the "Brauner Dogger" of Benken and is listed in Tab. 14. In addition, data for Weiach were obtained by H. N. Waber and are shown in Tab. 15. The XRD patterns are complex, especially when regarding the mixed layers. Pure smectite has never been detected. In the case of BEN 14, the mixed-layer phase is ordered, exhibiting a peak at an angle around 3° 2Θ. In samples BEN 11 and BEN 12 (Subfurcaten-Schichten), goethite was identified in the clay mineral fraction, but it is thought to be due to surficial oxidation.

Tab. 10: Benken: Results of mineralogical analyses

Lab ID	Depth [m]	Formation	Quartz [wt.-%]	K-feldspar [wt.-%]	Plagioclase [wt.-%]	Calcite [wt.-%]	Dol./Ank. [wt.-%]	Siderite [wt.-%]	Anhydrite [wt.-%]	Pyrite [wt.-%]	Clay min. [wt.-%]	Accessories	S [wt.-%]	C_{inorg} [wt.-%]	C_{org} [wt.-%]
BEN 1	395.97	Wohlgeschichtete Kalke	1	<1	<1	91	7	<1	<1	0.2	1		0.1	11.8	<0.1
BEN 2	407.38	Wohlgeschichtete Kalke	1	<1	<1	96	1	<1	<1	0.4	1		0.2	11.7	<0.1
BEN 3	417.83	Hornbuck-Schichten	2	<1	<1	85	5	<1	<1	0.2	9		0.1	10.8	<0.1
BEN 4	428.11	Hornbuck-Schichten	7	<1	<1	51	4	<1	<1	1.5	36		0.8	6.7	0.2
BEN 5	443.83	Effinger Schichten	5	<1	<1	78	2	<1	<1	1.3	13		0.7	9.7	0.1
BEN 6	459.90	Varians-Schichten	21	4	<1	20	<1	<1	<1	1.9	53		1.0	2.4	0.5
BEN 7	467.12	Parkinsoni-Württemb.-Sch.	22	2	<1	22	<1	1	<1	1.9	51		1.0	2.7	0.4
BEN 8	476.14	Parkinsoni-Württemb.-Sch.	17	3	<1	54	1	<1	<1	0.9	24		0.5	6.6	0.5
BEN 9	481.11	Parkinsoni-Württemb.-Sch.	15	3	<1	20	3	<1	<1	2.1	57		1.1	2.8	0.3
BEN 20	482.00	Parkinsoni-Württemb.-Sch.	20	4	<1	28	4	<1	<1	2.1	42		1.1	3.8	0.4
BEN 10	489.15	Parkinsoni-Württemb.-Sch.	20	4	1	19	2	<1	<1	2.1	52		1.1	2.5	0.3
BEN 11	498.61	Subfurcaten-Schichten	16	3	<1	45	1	<1	<1	1.1	34	Goethite	0.6	5.6	0.3
BEN 12	504.45	Subfurcaten-Schichten	19	1	<1	43	<1	<1	<1	0.7	36		0.4	5.1	0.4
BEN 13	507.87	Wedelsandstein-Formation	26	3	1	18	<1	<1	<1	1.7	50		0.9	2.1	0.3
BEN 21	525.45	Wedelsandstein-Formation	49	7	4	25	<1	<1	<1	0.6	14		0.3	3.0	0.2
BEN 14	525.88	Wedelsandstein-Formation	44	7	3	36	<1	<1	<1	0.6	10		0.3	4.3	0.4
BEN 15	535.49	Wedelsandstein-Formation	34	6	2	28	<1	<1	<1	1.1	29		0.6	3.3	0.4

Tab. 11: Riniken: Results of mineralogical analyses

Lab ID	Depth [m]	Formation	Quartz [wt.-%]	K-feldspar [wt.-%]	Plagioclase [wt.-%]	Calcite [wt.-%]	Dol./Ank. [wt.-%]	Siderite [wt.-%]	Anhydrite [wt.-%]	Pyrite [wt.-%]	Clay min. [wt.-%]	Accessories	S [wt.-%]	C_{inorg} [wt.-%]	C_{org} [wt.-%]
RIN 1	328.34	Murchisonae-Schichten	45	4	3	7	<1	<1	<1	1.1	40		0.6	0.8	0.3
RIN 2	334.68	Opalinuston	24	2	<1	26	<1	0	<1	3.4	44		1.8	3.2	0.7
RIN 3	344.72	Opalinuston	30	2	1	21	<1	1	<1	0.9	43		0.5	2.7	0.5
RIN 4	352.91	Opalinuston	23	2	1	12	<1	1	<1	1.5	59		0.8	1.5	0.6
RIN 5	365.03	Opalinuston	24	2	1	11	<1	2	<1	0.7	59		0.4	1.5	0.5
RIN 6	373.60	Opalinuston	22	2	1	17	<1	1	<1	1.7	54		0.9	2.2	0.5
RIN 7	385.16	Opalinuston	26	2	<1	11	1	2	<1	0.7	57		0.4	1.6	0.6
RIN 8	395.20	Opalinuston	21	2	1	8	0	2	<1	0.6	65		0.3	1.2	0.9
RIN 9	406.03	Opalinuston	30	3	<1	13	1	2	<1	0.7	50		0.4	1.9	0.3
RIN 10	416.28	Opalinuston	22	2	1	9	<1	2	<1	0.4	63		0.2	1.3	0.7
RIN 11	426.03	Opalinuston	17	1	<1	7	<1	4	<1	0.6	69		0.3	1.3	0.5
RIN 12	436.81	Opalinuston	14	1	<1	9	1	4	<1	0.6	71		0.3	1.5	0.6
RIN 13	446.51	Opalinuston	18	1	<1	11	<1	2	<1	1.1	65		0.6	1.6	0.5
RIN 14	455.84	Posidonienschiefer	10	<1	<1	29	1	<1	<1	4.3	48		2.3	3.6	7.6
RIN 15	466.07	Obtusus-Ton	60	4	1	13	5	<1	<1	3.6	13		1.9	2.2	0.5
RIN 16	476.25	Arietenkalk	45	4	1	8	2	<1	<1	0.9	39		0.5	1.2	0.6
RIN 17	485.67	Insektenmergel	19	2	<1	13	<1	<1	<1	5.4	60		2.9	1.5	1.0
RIN 18	487.70	Insektenmergel	24	3	<1	7	<1	<1	<1	0.7	66		0.4	0.8	<0.1

Tab. 12: Schafisheim: Results of mineralogical analyses

Lab ID	Depth [m]	Formation	Quartz [wt.-%]	K-feldspar [wt.-%]	Plagioclase [wt.-%]	Calcite [wt.-%]	Dol./Ank. [wt.-%]	Siderite [wt.-%]	Anhydrite [wt.-%]	Pyrite [wt.-%]	Clay min. [wt.-%]	Accessories	S [wt.-%]	C_{inorg} [wt.-%]	C_{org} [wt.-%]
SHA 1	963.05	Sowerbyi-Sauzei-Schichten	14	1	<1	57	<1	<1	<1	0.9	27		0.5	6.8	<0.1
SHA 2	974.32	Sowerbyi-Sauzei-Schichten	48	12	6	33	<1	<1	<1	0.6	2		0.3	3.9	0.1
SHA 3	985.03	Sowerbyi-Sauzei-Schichten	41	6	3	18	<1	<1	<1	0.9	30		0.5	2.2	0.2
SHA 4	994.20	Murchisonae-Schichten	56	7	1	26	5	<1	<1	0.4	5		0.2	3.8	0.3
SHA 5	1005.10	Opalinuston	24	2	<1	9	1	1	<1	2.1	60		1.1	1.4	0.2
SHA 6	1015.67	Opalinuston	30	4	1	11	1	1	<1	1.7	51		0.9	1.5	0.5
SHA 7	1026.11	Opalinuston	24	3	1	10	1	2	<1	0.6	58		0.3	1.6	<0.1
SHA 8	1035.75	Opalinuston	23	2	<1	7	1	2	<1	0.2	64		0.1	1.2	0.6
SHA 9	1046.03	Opalinuston	23	8	1	13	<1	2	<1	1.1	52		0.6	1.8	0.3
SHA 10	1056.63	Opalinuston	25	2	<1	10	1	3	<1	1.5	57		0.8	1.7	0.4
SHA 11	1063.95	Opalinuston	18	3	<1	13	<1	2	<1	1.7	61		0.9	1.8	0.3
SHA 12	1076.86	Opalinuston	24	2	<1	10	<1	2	<1	0.9	60		0.5	1.4	0.4
SHA 13	1087.78	Obtusus-Ton	41	<1	<1	21	7	<1	<1	1.1	30		0.6	3.4	0.2
SHA 14	1096.88	Insektenmergel	18	2	<1	11	<1	<1	<1	1.1	68		0.6	1.3	0.3
SHA 15	1105.10	Insektenmergel	16	2	<1	5	7	<1	<1	6.0	63	Gypsum	3.2	1.5	0.3
SHA 16	1117.57	Schilfsandstein	5	2	3	<1	32	<1	4	n.d.	53		1.0	4.2	0.4
SHA 17	1127.74	Schilfsandstein	21	13	6	<1	2	<1	<1	0.6	57		0.3	0.3	0.2
SHA 18	1138.08	Schilfsandstein	31	11	7	<1	2	<1	25	n.d.	24		5.8	0.3	0.3
SHA 19	1152.15	Gipskeuper	5	2	<1	<1	26	<1	12	n.d.	55		2.9	3.4	0.2
SHA 20	1162.05	Gipskeuper	1	<1	<1	<1	2	<1	86	n.d.	10		20.4	0.3	0.1
SHA 21	1173.84	Gipskeuper	11	<1	<1	<1	5	<1	71	n.d.	14		16.7	0.6	<0.1
SHA 22	1184.98	Gipskeuper	6	<1	<1	<1	28	<1	21	n.d.	45	Magnes. 3%, Smect.	5.0	3.6	<0.1
SHA 23	1196.99	Gipskeuper	5	1	<1	<1	18	<1	50	n.d.	27	Magnesite	11.7	2.3	<0.1
SHA 24	1208.68	Gipskeuper	4	4	<1	<1	12	<1	53	n.d.	27	Magnesite 1%	12.4	1.6	0.3
SHA 25	1218.59	Gipskeuper	1	<1	<1	<1	5	<1	93	n.d.	1		22.0	0.6	<0.1
SHA 26	1226.69	Lettenkohle	1	<1	<1	<1	99	<1	5	n.d.	0		1.2	12.9	<0.1
SHA 27	1234.28	Trigonodus-Dolomit	1	<1	<1	<1	92	<1	3	n.d.	4		0.8	11.9	<0.1

Tab. 13: Weiach: Results of mineralogical analyses
Data for samples WEI 1 to WEI 22 are from H. N. Waber

Lab ID	Depth [m]	Formation	Quartz [wt.-%]	K-feldspar [wt.-%]	Plagioclase [wt.-%]	Calcite [wt.-%]	Dol./Ank. [wt.-%]	Siderite [wt.-%]	Anhydrite [wt.-%]	Pyrite [wt.-%]	Clay min. [wt.-%]	Accessories	S [wt.-%]	C_{inorg} [wt.-%]	C_{org} [wt.-%]
WEI 31	271.98	Massenkalk	3	<1	<1	79	<1	<1	<1	1.5	16	Gypsum	0.8	9.5	0.4
WEI 32	285.77	Quaderkalk	9	<1	<1	66	<1	<1	<1	0.4	24		0.2	7.9	0.4
WEI 33	299.52	Schwarzbach-Schichten	4	<1	<1	75	6	<1	<1	0.4	15		0.2	9.7	0.1
WEI 34	309.33	Schwarzbach-Schichten	7	<1	<1	52	5	<1	<1	1.1	34		0.6	6.9	0.2
WEI 35	320.25	Wangental-Schichten	3	<1	<1	83	<1	<1	<1	0.6	14		0.3	9.9	<0.1
WEI 36	330.06	Wangental-Schichten	2	<1	<1	97	<1	<1	<1	0.4	1		0.2	11.6	<0.1
WEI 37	330.88	Wangental-Schichten	<1	<1	<1	96	<1	<1	<1	0.4	4		0.2	11.5	<0.1
WEI 25	340.51	Küssaburg-Schichten	3	<1	<1	83	2	<1	<1	0.4	11		0.2	10.2	0.1
WEI 38	351.14	Küssaburg-Schichten	1	<1	<1	95	3	<1	<1	0.2	1		0.1	11.7	<0.1
WEI 39	362.41	Küssaburg-Schichten	2	<1	<1	90	3	<1	<1	0.4	4		0.2	11.2	<0.1
WEI 40	374.73	Küssaburg-Schichten	3	<1	<1	84	2	<1	<0.4	<0.2	11		<0.1	10.3	<0.1
WEI 41	386.05	Hornbuck-Schichten	4	<1	<1	72	3	<1	<1	1.3	20		0.7	9.0	<0.1
WEI 42	394.91	Effinger Schichten	7	<1	<1	73	3	<1	<1	0.2	17		0.1	9.1	<0.1
WEI 43	404.98	Effinger Schichten	9	1	<1	69	3	<1	<1	0.7	17		0.4	8.7	<0.1
WEI 44	415.79	Effinger Schichten	7	<1	<1	78	2	<1	<1	0.7	12		0.4	9.6	<0.1
WEI 45	426.14	Effinger Schichten	6	<1	<1	69	2	<1	<1	0.6	21		0.3	8.6	0.5
WEI 46	436.39	Effinger Schichten	6	<1	<1	52	1	<1	<1	0.9	39		0.5	6.4	0.7
WEI 47	450.30	Effinger Schichten	6	1	<1	67	<1	<1	<1	0.9	26		0.5	8.0	0.1
WEI 48	459.69	Effinger Schichten	11	1	<1	66	<1	<1	<1	0.9	21		0.5	7.9	0.2
WEI 49	467.84	Effinger Schichten	6	<1	<1	71	<1	<1	<1	0.9	22		0.5	8.5	<0.1
WEI 50	476.09	Effinger Schichten	8	1	<1	71	<1	<1	<1	0.2	20		0.1	8.5	0.1
WEI 1	484.14	Varians-Schichten	15	2	0	12	1	<1	<1	2.8	66		1.5	1.6	0.5
WEI 2	495.46	Württembergica-Schichten	19	5	1	27	1	<1	<1	2.8	44		1.5	3.4	0.1
WEI 3	506.08	Württembergica-Schichten	16	3	1	27	1	<1	<1	2.4	49		1.3	3.4	0.2
WEI 4	517.10	Württembergica-Schichten	15	2	1	21	2	<1	<1	3.2	56		1.7	2.7	0.1
WEI 5	527.86	Parkinsoni-Schichten	27	3	1	29	<1	<1	<1	0.9	39		0.5	3.5	0.0
WEI 6	539.26	Sowerbyi-Sauzei-Schichten	17	2	0	23	<1	<1	<1	1.3	56		0.7	2.8	0.2
WEI 7	549.62	Murchisonae-Schichten	19	2	2	5	<1	<1	<1	1.9	70		1.0	0.6	0.1
WEI 51	560.48	Opalinuston	27	3	<1	53	<1	<1	<1	0.6	17		0.3	6.3	<0.1
WEI 8	561.08	Opalinuston	27	3	1	20	1	<1	<1	1.7	45		0.9	2.6	0.4
WEI 9	572.80	Opalinuston	18	2	1	12	<1	<1	<1	3.7	63		2.0	1.4	0.6
WEI 52	581.86	Opalinuston	33	4	1	19	<1	<1	<1	2.1	40		1.1	2.3	0.6
WEI 10	582.04	Opalinuston	23	3	0	12	<1	<1	<1	0.7	61		0.4	1.4	0.6
WEI 11	594.74	Opalinuston	23	3	0	8	<1	<1	<1	0.6	64		0.3	1.0	1.1
WEI 12	605.34	Opalinuston	20	2	0	11	<1	<1	<1	0.6	66		0.3	1.3	0.8
WEI 13	616.32	Opalinuston	21	3	1	12	<1	<1	<1	0.6	62		0.3	1.4	0.8
WEI 14	627.09	Opalinuston	16	2	0	13	<1	<1	<1	14.4	54		7.7	1.6	0.0
WEI 15	638.09	Opalinuston	19	2	0	10	<1	<1	<1	0.4	68		0.2	1.2	0.9
WEI 16	649.46	Opalinuston	16	2	0	12	<1	<1	<1	1.1	68		0.6	1.4	0.9
WEI 53	652.20	Opalinuston	10	1	<1	9	<1	1	<1	2.6	75		1.4	1.2	0.9
WEI 17	660.30	Opalinuston	15	2	0	12	<1	<1	<1	0.9	70		0.5	1.4	0.6
WEI 18	671.89	Posidonienschiefer	6	1	1	46	1	<1	<1	2.8	38		1.5	5.7	3.7
WEI 19	682.16	Obtusus-Ton	45	4	2	7	4	<1	<1	2.4	35		1.3	1.4	0.7
WEI 20	693.19	Obtusus-Ton	29	3	1	12	2	<1	<1	3.9	49		2.1	1.6	0.5
WEI 21	703.88	Insektenmergel	12	2	0	23	<1	<1	<1	1.7	60		0.9	2.8	0.5
WEI 22	715.56	Knollenmergel	9	2	3	19	21	<1	<1	0.0	45		0.0	5.1	0.4
WEI 54	723.98	Obere Bunte Mergel	9	5	3	<1	28	<1	<0.4	<0.2	55	Hematite	<0.1	3.7	<0.1
WEI 55	736.12	Schilfsandstein	6	6	1	<1	<1	3	<1	0.4	84		0.2	0.3	<0.1
WEI 56	744.63	Gipskeuper	9	2	<1	14	18	<1	3	n.d.	54		0.6	4.1	<0.1
WEI 57	757.94	Gipskeuper	33	6	5	<1	26	<1	4	n.d.	26	Ilmenite?	0.9	3.4	0.2
WEI 58	769.10	Gipskeuper	3	<1	<1	<1	13	<1	73	n.d.	10		17.3	1.7	<0.1
WEI 59	782.38	Gipskeuper	10	<1	<1	<1	24	<1	36	n.d.	30		8.6	3.1	<0.1
WEI 60	790.71	Gipskeuper	11	3	<1	<1	20	<1	9	n.d.	57	Gypsum 3%	2.1	2.6	<0.1
WEI 61	802.29	Gipskeuper	2	3	<1	<1	25	<1	29	n.d.	42	Gypsum	6.8	3.2	<0.1
WEI 62	812.25	Gipskeuper	1	<1	<1	<1	39	<1	58	n.d.	1		13.8	5.1	<0.1
WEI 63	818.50	Lettenkohle	22	18	<1	<1	8	<1	<1	4.3	48	Gypsum	2.3	1.0	0.4

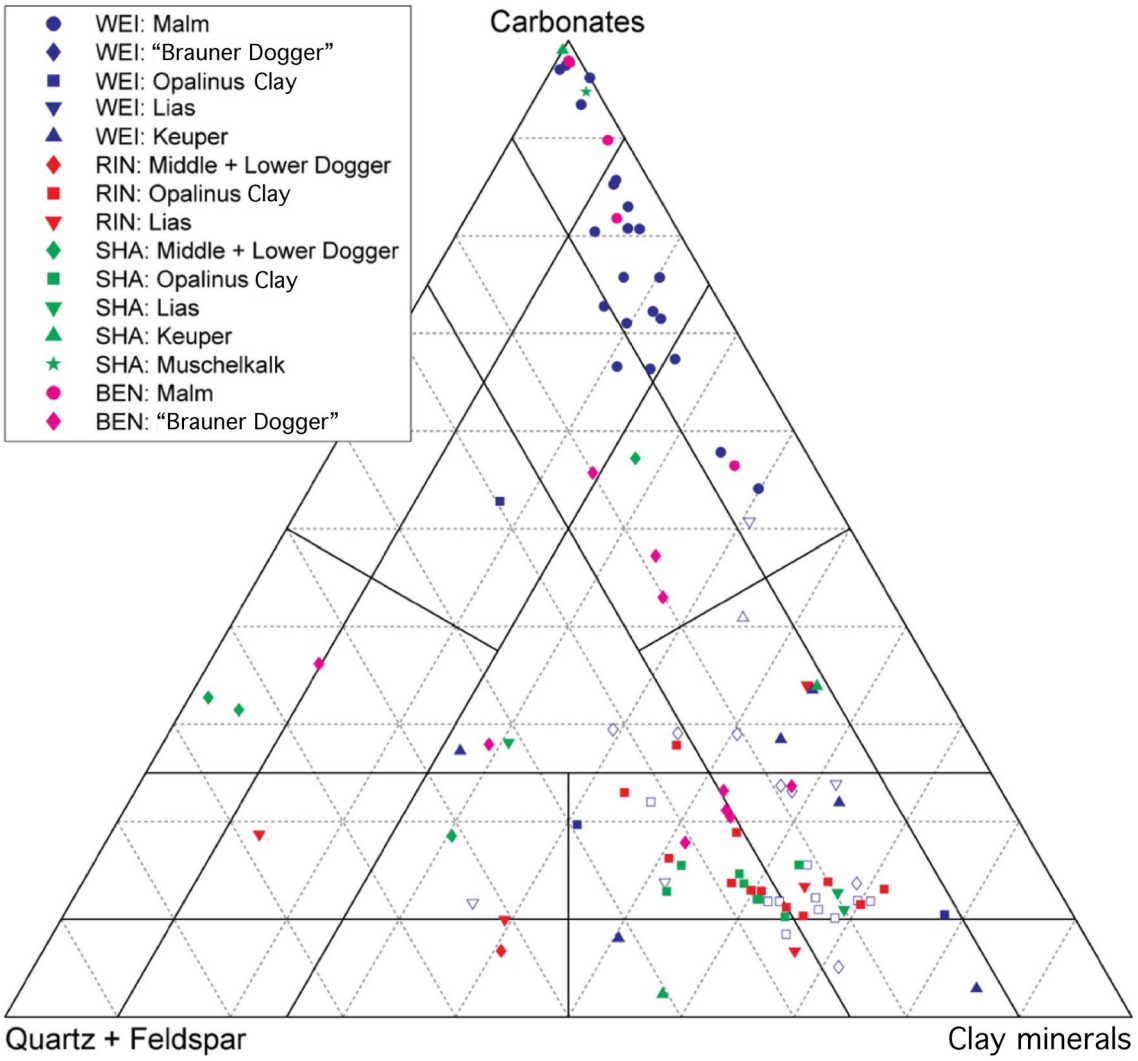

Fig. 5: Mineralogy in a ternary plot after Füchtbauer (1988)

Empty symbols for Weiach represent data from H. N. Waber. Evaporites with >10 % anhydrite are not shown

Tab. 14: Benken: Results of analyses of clay mineralogy

Data refer to weight fractions in the total rock. Ill./smec. ML: Illite-smectite mixed layers

Lab ID	Depth [m]	Formation	Illite [wt.-%]	Ill./smec. ML [wt.-%]	Chlorite [wt.-%]	Kaolinite [wt.-%]
BEN 5	443.83	Effinger Schichten	3	5	1	4
BEN 6	459.90	Varians-Schichten	10	16	5	23
BEN 7	467.12	Parkinsoni-Württemb.-Sch.	10	16	3	21
BEN 8	476.14	Parkinsoni-Württemb.-Sch.	5	8	2	10
BEN 9	481.11	Parkinsoni-Württemb.-Sch.	11	18	5	22
BEN 20	482.00	Parkinsoni-Württemb.-Sch.	10	14	4	15
BEN 10	489.15	Parkinsoni-Württemb.-Sch.	10	18	5	19
BEN 11	498.61	Subfurcaten-Schichten	4	10	3	16
BEN 12	504.45	Subfurcaten-Schichten	6	14	3	14
BEN 21	525.45	Wedelsandstein-Formation	2	5	5	2
BEN 14	525.88	Wedelsandstein-Formation	1	3	1	4

Tab. 15: Weiach: Results of analyses of clay mineralogy

Data of H. N. Waber. Data refer to weight fractions in the total rock. Ill./smec. ML: Illite-smectite mixed layers

Lab ID	Depth [m]	Formation	Illite [wt.-%]	Ill./smec. ML [wt.-%]	Chlorite [wt.-%]	Kaolinite [wt.-%]
WEI 1	484.14	Varians-Schichten	22	18	2	24
WEI 2	495.46	Württembergica-Schichten	20	14	1	9
WEI 3	506.08	Württembergica-Schichten	17	16	3	12
WEI 4	517.10	Württembergica-Schichten	22	16	2	16
WEI 5	527.86	Parkinsoni-Schichten	13	19	2	4
WEI 6	539.26	Sowerbyi-Sauzei-Schichten	18	15	5	19
WEI 7	549.62	Murchisonae-Schichten	24	25	3	19
WEI 8	561.08	Opalinuston	15	12	3	16
WEI 9	572.80	Opalinuston	19	15	4	24
WEI 10	582.04	Opalinuston	18	16	4	23
WEI 11	594.74	Opalinuston	16	29	3	15
WEI 12	605.34	Opalinuston	17	26	4	18
WEI 13	616.32	Opalinuston	16	24	3	19
WEI 14	627.09	Opalinuston	15	17	4	18
WEI 15	638.09	Opalinuston	21	17	7	22
WEI 16	649.46	Opalinuston	20	21	5	23
WEI 17	660.30	Opalinuston	23	16	7	23
WEI 18	671.89	Posidonienschiefer	15	9	4	10
WEI 19	682.16	Obtusus-Ton	12	8	5	11
WEI 20	693.19	Obtusus-Ton	19	13	3	14
WEI 21	703.88	Insektenmergel	26	21	4	9
WEI 22	715.56	Knollenmergel	23	21	0	0

4.2 Densities and physical porosity

The measured bulk dry and grain densities and calculated physical porosities are listed in Tab. 16 - 19. Routinely, two measurements (on different rock materials) of bulk dry and grain densities were performed per sample, and the average is listed and used for further calculations. If the standard deviation between these measurements exceeded 0.04 g/cm^3, another measurement was made. Some samples still show a high variability (*e.g.* in the Gipskeuper of Schafisheim and Weiach). This scatter reflects the lithological heterogeneity on the scale of the sample size and not analytical problems. Note that the error on physical porosity listed in Tab. 16 - 19 relates exclusively to the analytical uncertainty on the density measurements and is around 1.6 % irrespective of the porosity value. In low-porosity rocks (<5 %), the relative error on porosity calculated from densities becomes large, and the data need to be interpreted with care. The additional uncertainty related to sample heterogeneity is taken into account in the data-screening procedure (Section 6.2).

A set of samples from Weiach was studied previously by H. N. Waber. Since then, the sample materials have been stored at room temperature in the Institute of Geological Sciences at Bern over several years. These materials were used again in this study for the density measurements. However, the samples showed extensive oxidation phenomena and were crumbly, in particular the clay-rich lithiologies. Some of the porosities calculated from the data were aberrantly high. It appears that the long-term storage of unprotected samples under indoor conditions led to a stronger deterioration when compared to samples taken from intact core materials sealed into plastic sleeves. Therefore, the new density data produced on Waber's samples are not considered trustworthy and were eliminated from the data base.

Tab. 16: Benken: Densities and physical porosity

n: number of density measurements per sample; Variability: Standard deviation of individual density measurements; Error: Propagated error on physical porosity, assuming a total analytical error of ±1.2 % for bulk dry density and ± 1.3 % for grain density measurements (see Section 3.2)

Lab ID	Depth [m]	Formation	Bulk dry density [g/cm^3]	n	Variability [g/cm^3]	Grain density [g/cm^3]	n	Variability [g/cm^3]	Physical porosity [%]	Error [%]
BEN 1	395.97	Wohlgeschichtete Kalke	2.60	2	0.01	2.69	2	0.01	3.3	1.7
BEN 2	407.38	Wohlgeschichtete Kalke	2.65	2	0.03	2.76	2	0.02	3.9	1.7
BEN 3	417.83	Hornbuck-Schichten	2.59	3	0.03	2.70	3	0.05	4.2	1.7
BEN 4	428.11	Hornbuck-Schichten	2.48	2	0.02	2.74	2	0.00	9.5	1.6
BEN 5	443.83	Effinger Schichten	2.52	2	0.00	2.76	2	0.01	8.8	1.6
BEN 6	459.90	Varians-Schichten	2.37	2	0.00	2.69	3	0.03	11.9	1.6
BEN 7	467.12	Parkinsoni-Württemb.-Sch.	2.37	2	0.03	2.72	2	0.02	12.7	1.5
BEN 8	476.14	Parkinsoni-Württemb.-Sch.	2.51	2	0.00	2.66	2	0.01	5.8	1.7
BEN 9	481.11	Parkinsoni-Württemb.-Sch.	2.36	2	0.00	2.72	2	0.02	13.1	1.5
BEN 20	482.00	Parkinsoni-Württemb.-Sch.	2.39	2	0.01	2.71	2	0.01	11.9	1.6
BEN 10	489.15	Parkinsoni-Württemb.-Sch.	2.38	2	0.03	2.72	2	0.01	12.2	1.6
BEN 11	498.61	Subfurcaten-Schichten	2.40	4	0.08	2.80	3	0.05	14.3	1.5
BEN 12	504.45	Subfurcaten-Schichten	2.40	2	0.04	2.74	2	0.01	12.4	1.5
BEN 13	507.87	Wedelsandstein-Formation	2.33	3	0.05	2.72	2	0.00	14.1	1.5
BEN 21	525.45	Wedelsandstein-Formation	2.37	2	0.00	2.68	2	0.01	11.7	1.6
BEN 14	525.88	Wedelsandstein-Formation	2.45	3	0.04	2.67	2	0.01	8.1	1.6
BEN 15	535.49	Wedelsandstein-Formation	2.42	2	0.01	2.68	2	0.00	9.8	1.6

Tab. 17: Riniken: Densities and physical porosity

n: number of density measurements per sample; Variability: Standard deviation of individual density measurements; Error: Propagated error on physical porosity, assuming a total analytical error of ±1.2 % for bulk dry density and ± 1.3 % for grain density measurements (see Section 3.2)

Lab ID	Depth [m]	Formation	Bulk dry density [g/cm³]	n	Variability [g/cm³]	Grain density [g/cm³]	n	Variability [g/cm³]	Physical porosity [%]	Error [%]
RIN 1	328.34	Murchisonae-Schichten	2.40	2	0.00	2.72	2	0.03	11.6	1.6
RIN 2	334.68	Opalinuston	2.50	2	0.03	2.70	2	0.01	7.6	1.6
RIN 3	344.72	Opalinuston	2.41	2	0.02	2.68	3	0.03	10.3	1.6
RIN 4	352.91	Opalinuston	2.46	2	0.01	2.70	2	0.00	8.8	1.6
RIN 5	365.03	Opalinuston	2.40	2	0.03	2.70	2	0.02	11.0	1.6
RIN 6	373.60	Opalinuston	2.43	2	0.02	2.70	2	0.00	10.0	1.6
RIN 7	385.16	Opalinuston	2.41	2	0.01	2.73	2	0.03	11.7	1.6
RIN 8	395.20	Opalinuston	2.41	2	0.01	2.72	2	0.03	11.4	1.6
RIN 9	406.03	Opalinuston	2.45	3	0.05	2.73	2	0.02	10.2	1.6
RIN 10	416.28	Opalinuston	2.42	2	0.01	2.70	2	0.00	10.3	1.6
RIN 11	426.03	Opalinuston	2.45	3	0.04	2.74	2	0.02	10.5	1.6
RIN 12	436.81	Opalinuston	2.41	2	0.01	2.72	2	0.02	11.6	1.6
RIN 13	446.51	Opalinuston	2.42	2	0.03	2.72	2	0.02	10.9	1.6
RIN 14	455.84	Posidonienschiefer	2.24	2	0.02	2.48	2	0.00	9.7	1.6
RIN 15	466.07	Obtusus-Ton	2.48	2	0.00	2.78	2	0.02	10.9	1.6
RIN 16	476.25	Arietenkalk	2.45	2	0.00	2.68	2	0.00	8.9	1.6
RIN 17	485.67	Insektenmergel	2.43	3	0.06	2.74	3	0.04	11.3	1.6
RIN 18	487.70	Insektenmergel	2.33	2	0.01	2.68	2	0.02	13.3	1.5

Tab. 18: Schafisheim: Densities and physical porosity

n: number of density measurements per sample; Variability: Standard deviation of individual density measurements; Error: Propagated error on physical porosity, assuming a total analytical error of ±1.2 % for bulk dry density and ± 1.3 % for grain density measurements (see Section 3.2)

Lab ID	Depth [m]	Formation	Bulk dry density [g/cm³]	n	Variability [g/cm³]	Grain density [g/cm³]	n	Variability [g/cm³]	Physical porosity [%]	Error [%]
SHA 1	963.05	Sowerbyi-Sauzei-Schichten	2.56	2	0.00	2.72	2	0.04	6.0	1.7
SHA 2	974.32	Sowerbyi-Sauzei-Schichten	2.57	2	0.04	2.69	2	0.00	4.5	1.7
SHA 3	985.03	Sowerbyi-Sauzei-Schichten	2.56	2	0.01	2.78	2	0.02	7.6	1.6
SHA 4	994.20	Murchisonae-Schichten	2.56	2	0.02	2.75	2	0.02	6.7	1.7
SHA 5	1005.10	Opalinuston	2.51	2	0.02	2.78	2	0.03	9.6	1.6
SHA 6	1015.67	Opalinuston	2.50	2	0.00	2.70	2	0.01	7.4	1.6
SHA 7	1026.11	Opalinuston	2.50	2	0.02	2.78	2	0.02	10.1	1.6
SHA 8	1035.75	Opalinuston	2.47	2	0.01	2.68	2	0.00	8.1	1.6
SHA 9	1046.03	Opalinuston	2.51	2	0.03	2.73	2	0.02	8.2	1.6
SHA 10	1056.63	Opalinuston	2.48	2	0.01	2.69	2	0.01	8.0	1.6
SHA 11	1063.95	Opalinuston	2.51	2	0.01	2.68	2	0.01	6.3	1.7
SHA 12	1076.86	Opalinuston	2.54	2	0.02	2.69	2	0.01	5.8	1.7
SHA 13	1087.78	Obtusus-Ton	2.58	2	0.01	2.73	2	0.01	5.3	1.7
SHA 14	1096.88	Insektenmergel	2.44	2	0.01	2.73	2	0.00	10.6	1.6
SHA 15	1105.10	Insektenmergel	2.41	2	0.00	2.69	3	0.06	10.2	1.6
SHA 16	1117.57	Schilfsandstein	2.51	2	0.00	2.82	2	0.00	10.9	1.6
SHA 17	1127.74	Schilfsandstein	2.45	2	0.02	2.68	2	0.03	8.6	1.6
SHA 18	1138.08	Schilfsandstein	2.58	2	0.01	2.70	2	0.00	4.3	1.7
SHA 19	1152.15	Gipskeuper	2.50	2	0.00	2.82	2	0.02	11.4	1.6
SHA 20	1162.05	Gipskeuper	2.88	2	0.01	2.94	3	0.04	2.1	1.7
SHA 21	1173.84	Gipskeuper	2.77	2	0.03	2.96	2	0.01	6.4	1.7
SHA 22	1184.98	Gipskeuper	2.56	3	0.20	2.82	2	0.01	9.0	1.6
SHA 23	1196.99	Gipskeuper	2.78	3	0.02	2.87	2	0.00	3.3	1.7
SHA 24	1208.68	Gipskeuper	2.70	3	0.10	2.88	2	0.01	6.1	1.7
SHA 25	1218.59	Gipskeuper	2.93	2	0.02	2.98	2	0.02	1.6	1.7
SHA 26	1226.69	Lettenkohle	2.81	2	0.01	2.87	3	0.02	1.8	1.7
SHA 27	1234.28	Trigonodus-Dolomit	2.59	3	0.06	2.85	2	0.02	9.0	1.6

Tab. 19: Weiach: Densities and physical porosity

n: number of density measurements per sample; Variability: Standard deviation of individual density measurements; Error: Propagated error on physical porosity, assuming a total analytical error of ±1.2 % for bulk dry density and ± 1.3 % for grain density measurements (see Section 3.2)

Lab ID	Depth [m]	Formation	Bulk dry density [g/cm³]	n	Variability [g/cm³]	Grain density [g/cm³]	n	Variability [g/cm³]	Physical porosity [%]	Error [%]
WEI 31	271.98	Massenkalk	2.50	2	0.01	2.73	2	0.01	8.4	1.6
WEI 32	285.77	Quaderkalk	2.49	2	0.02	2.69	2	0.02	7.4	1.6
WEI 33	299.52	Schwarzbach-Schichten	2.61	2	0.00	2.68	2	0.01	2.8	1.7
WEI 34	309.33	Schwarzbach-Schichten	2.45	2	0.00	2.69	2	0.01	9.2	1.6
WEI 35	320.25	Wangental-Schichten	2.54	2	0.01	2.71	2	0.00	6.1	1.7
WEI 36	330.06	Wangental-Schichten	2.66	2	0.01	2.70	2	0.01	1.7	1.7
WEI 37	330.88	Wangental-Schichten	2.68	2	0.01	2.72	2	0.02	1.5	1.7
WEI 25	340.51	Küssaburg-Schichten	2.56	2	0.00	2.69	2	0.01	5.0	1.7
WEI 38	351.14	Küssaburg-Schichten	2.64	2	0.03	2.69	2	0.00	1.8	1.7
WEI 39	362.41	Küssaburg-Schichten	2.60	2	0.01	2.70	2	0.01	3.8	1.7
WEI 40	374.73	Küssaburg-Schichten	2.56	2	0.01	2.70	2	0.02	5.2	1.7
WEI 41	386.05	Hornbuck-Schichten	2.51	2	0.00	2.73	2	0.03	7.9	1.6
WEI 42	394.91	Effinger Schichten	2.52	2	0.01	2.71	2	0.03	7.1	1.6
WEI 43	404.98	Effinger Schichten	2.54	2	0.02	2.72	2	0.01	6.9	1.6
WEI 44	415.79	Effinger Schichten	2.56	2	0.01	2.71	2	0.02	5.7	1.7
WEI 45	426.14	Effinger Schichten	2.56	2	0.00	2.74	2	0.02	6.8	1.6
WEI 46	436.39	Effinger Schichten	2.47	2	0.01	2.73	2	0.01	9.5	1.6
WEI 47	450.30	Effinger Schichten	2.51	2	0.02	2.74	2	0.01	8.6	1.6
WEI 48	459.69	Effinger Schichten	2.50	2	0.01	2.73	2	0.01	8.2	1.6
WEI 49	467.84	Effinger Schichten	2.54	2	0.00	2.71	2	0.02	6.2	1.7
WEI 50	476.09	Effinger Schichten	2.55	2	0.01	2.71	2	0.00	5.9	1.7
WEI 51	560.48	Opalinuston	2.52	2	0.02	2.74	2	0.01	7.8	1.6
WEI 52	581.86	Opalinuston	2.47	2	0.02	2.69	2	0.02	8.1	1.6
WEI 53	652.20	Opalinuston	2.39	2	0.02	2.68	2	0.00	10.7	1.6
WEI 54	723.98	Obere Bunte Mergel	2.42	2	0.02	2.78	2	0.00	13.1	1.5
WEI 55	736.12	Schilfsandstein	2.34	2	0.01	2.77	3	0.03	15.5	1.5
WEI 56	744.63	Gipskeuper	2.43	2	0.03	2.75	2	0.01	11.8	1.6
WEI 57	757.94	Gipskeuper	2.57	2	0.02	2.75	2	0.00	6.6	1.7
WEI 58	769.10	Gipskeuper	2.90	2	0.01	2.90	2	0.02	b.d.	1.8
WEI 59	782.38	Gipskeuper	2.78	2	0.02	2.86	2	0.03	3.1	1.7
WEI 60	790.71	Gipskeuper	2.42	3	0.10	2.77	2	0.01	12.5	1.5
WEI 61	802.29	Gipskeuper	2.59	3	0.09	2.81	2	0.03	8.0	1.6
WEI 62	812.25	Gipskeuper	2.81	3	0.10	2.91	2	0.00	3.4	1.7
WEI 63	818.50	Lettenkohle	2.47	3	0.04	2.65	2	0.01	6.8	1.6

4.3 Anion concentrations

Anion concentrations obtained from aqueous extractions are reported in Tab. 20 - 23. All data are given in units of mass per $L_{solution}$, which, at the chosen solid:liquid mass ratio of 1, corresponds to mass per kg_{rock}. Reported values are averages of duplicate measurements.

Measured SO_4^{2-} concentrations are high but most probably not representative of *in-situ* pore water. Given the long-term storage of the samples under atmospheric conditions and the fact that the extractions were prepared under ambient laboratory conditions, SO_4^{2-} is strongly affected by pyrite oxidation. In anhydrite-bearing samples (mainly Gipskeuper), anhydrite

dissolution is another source of SO_4^{2-}. I^- contents in pore waters of marine sedimentary rocks are typically much higher than in sea water because the main contribution originates from the decomposition of organic matter during diagenesis (see also Mazurek *et al.* 2011). Thus, because I^- is not strictly conservative and depends on the nature and concentration of organic matter, it is not considered here any further. Therefore, further use of anion concentrations is limited to chloride ±bromide.

Tab. 20: Benken: Anion concentration in aqueous leachate solutions

Cl^-, SO_4^{--}: Analysed by ion chromatography; Br^-, I^-: Analysed by ICP-MS (British Geological Survey, Keyworth, UK)

Lab ID	Depth [m]	Formation	Cl^- in leachate [mg/L]	SO_4^{--} in leachate [mg/L]	Br^- in leachate [µg/L]	I^- in leachate [µg/L]
BEN 1	395.97	Wohlgeschichtete Kalke	66	320	301	52.9
BEN 2	407.38	Wohlgeschichtete Kalke	38	219	215	121.9
BEN 3	417.83	Hornbuck-Schichten	48	618	143	114.9
BEN 4	428.11	Hornbuck-Schichten	117	2053	<91	19.6
BEN 5	443.83	Effinger Schichten	89	607	191	205.4
BEN 6	459.90	Varians-Schichten	174	1445	<91	7.7
BEN 7	467.12	Parkinsoni-Württemb.-Sch.	174	1381	<91	10.1
BEN 8	476.14	Parkinsoni-Württemb.-Sch.	110	672	<91	37.5
BEN 9	481.11	Parkinsoni-Württemb.-Sch.	195	1434	<91	10.8
BEN 20	482.00	Parkinsoni-Württemb.-Sch.	n.d.	n.d.	n.d.	n.d.
BEN 10	489.15	Parkinsoni-Württemb.-Sch.	179	1375	<91	10.8
BEN 11	498.61	Subfurcaten-Schichten	376	938	341	71.0
BEN 12	504.45	Subfurcaten-Schichten	258	781	187	136.7
BEN 13	507.87	Wedelsandstein-Formation	177	1567	<91	10.1
BEN 21	525.45	Wedelsandstein-Formation	n.d.	n.d.	n.d.	n.d.
BEN 14	525.88	Wedelsandstein-Formation	180	1721	<91	19.7
BEN 15	535.49	Wedelsandstein-Formation	125	2047	<91	16.9

Tab. 21: Riniken: Anion concentration in aqueous leachate solutions

Cl^-, SO_4^{--}: Analysed by ion chromatography; Br^-, I^-: Analysed by ICP-MS (British Geological Survey, Keyworth, UK)

Lab ID	Depth [m]	Formation	Cl^- in leachate [mg/L]	SO_4^{--} in leachate [mg/L]	Br^- in leachate [µg/L]	I^- in leachate [µg/L]
RIN 1	328.34	Murchisonae-Schichten	72	1703	<91	4.7
RIN 2	334.68	Opalinuston	76	1811	<91	19.9
RIN 3	344.72	Opalinuston	73	1053	140	9.0
RIN 4	352.91	Opalinuston	72	1674	166	6.8
RIN 5	365.03	Opalinuston	66	791	151	5.8
RIN 6	373.60	Opalinuston	56	1656	167	8.3
RIN 7	385.16	Opalinuston	57	849	162	6.0
RIN 8	395.20	Opalinuston	60	1498	207	4.0
RIN 9	406.03	Opalinuston	61	1354	149	5.4
RIN 10	416.28	Opalinuston	64	1046	160	5.3
RIN 11	426.03	Opalinuston	62	807	119	6.4
RIN 12	436.81	Opalinuston	74	1094	161	5.5
RIN 13	446.51	Opalinuston	61	1362	107	5.9
RIN 14	455.84	Posidonienschiefer	78	2027	<91	16.0
RIN 15	466.07	Obtusus-Ton	47	1592	<91	10.0
RIN 16	476.25	Arietenkalk	52	1155	<91	8.1
RIN 17	485.67	Insektenmergel	60	1842	<91	13.6
RIN 18	487.70	Insektenmergel	47	2077	<91	0.8

Tab. 22: Schafisheim: Anion concentration in aqueous leachate solutions

Cl^-, SO_4^{--}: Analysed by ion chromatography; Br^-, I^-: Analysed by ICP-MS (British Geological Survey, Keyworth, UK)

Lab ID	Depth [m]	Formation	Cl^- in leachate [mg/L]	SO_4^{--} in leachate [mg/L]	Br^- in leachate [µg/L]	I^- in leachate [µg/L]
SHA 1	963.05	Sowerbyi-Sauzei-Schichten	139	1576	356	275.3
SHA 2	974.32	Sowerbyi-Sauzei-Schichten	179	1063	433	57.8
SHA 3	985.03	Sowerbyi-Sauzei-Schichten	131	719	331	5.1
SHA 4	994.20	Murchisonae-Schichten	284	1285	919	14.8
SHA 5	1005.10	Opalinuston	217	989	638	4.8
SHA 6	1015.67	Opalinuston	187	1472	589	5.9
SHA 7	1026.11	Opalinuston	196	841	705	6.6
SHA 8	1035.75	Opalinuston	204	578	680	6.9
SHA 9	1046.03	Opalinuston	213	1752	693	7.0
SHA 10	1056.63	Opalinuston	264	979	890	11.7
SHA 11	1063.95	Opalinuston	195	766	593	10.8
SHA 12	1076.86	Opalinuston	161	579	518	8.5
SHA 13	1087.78	Obtusus-Ton	71	267	233	53.1
SHA 14	1096.88	Insektenmergel	249	1130	669	15.4
SHA 15	1105.10	Insektenmergel	204	3000	480	14.5
SHA 16	1117.57	Schilfsandstein	378	1924	1539	5.9
SHA 17	1127.74	Schilfsandstein	393	2012	1194	7.4
SHA 18	1138.08	Schilfsandstein	245	1951	558	6.4
SHA 19	1152.15	Gipskeuper	241	1443	902	8.1
SHA 20	1162.05	Gipskeuper	42	1937	132	1.2
SHA 21	1173.84	Gipskeuper	89	2034	361	0.9
SHA 22	1184.98	Gipskeuper	275	1222	1321	4.6
SHA 23	1196.99	Gipskeuper	173	1925	784	4.5
SHA 24	1208.68	Gipskeuper	286	1967	1738	6.3
SHA 25	1218.59	Gipskeuper	10	1761	<91	0.9
SHA 26	1226.69	Lettenkohle	191	2030	2425	24.5
SHA 27	1234.28	Trigonodus-Dolomit	253	2044	562	7.8

Tab. 23: Weiach: Anion concentration in aqueous leachate solutions

Data for samples WEI 1 to WEI 22 are from H. N. Waber. Cl^-, SO_4^{--}: Analysed by ion chromatography; Br^-, I^-: Analysed by ICP-MS (British Geological Survey, Keyworth, UK)

Lab ID	Depth [m]	Formation	Cl^- in leachate [mg/L]	SO_4^{--} in leachate [mg/L]	Br^- in leachate [µg/L]	I^- in leachate [µg/L]
WEI 31	271.98	Massenkalk	51	1958	<91	16.8
WEI 32	285.77	Quaderkalk	66	1973	95	34.0
WEI 33	299.52	Schwarzbach-Schichten	65	810	149	81.6
WEI 34	309.33	Schwarzbach-Schichten	107	2014	<91	21.4
WEI 35	320.25	Wangental-Schichten	67	1808	93	25.7
WEI 36	330.06	Wangental-Schichten	43	631	269	154.4
WEI 37	330.88	Wangental-Schichten	20	313	177	134.9
WEI 25	340.51	Küssaburg-Schichten	63	1015	216	88.2
WEI 38	351.14	Küssaburg-Schichten	41	1243	175	108.7
WEI 39	362.41	Küssaburg-Schichten	48	1620	151	41.1
WEI 40	374.73	Küssaburg-Schichten	62	1532	104	64.1
WEI 41	386.05	Hornbuck-Schichten	82	1945	<91	39.0
WEI 42	394.91	Effinger Schichten	71	1996	105	75.7
WEI 43	404.98	Effinger Schichten	64	1496	184	136.2
WEI 44	415.79	Effinger Schichten	64	>3000	211	338.8
WEI 45	426.14	Effinger Schichten	62	1512	252	214.7
WEI 46	436.39	Effinger Schichten	111	2015	201	121.2
WEI 47	450.30	Effinger Schichten	88	1748	359	376.1
WEI 48	459.69	Effinger Schichten	80	1697	289	341.8
WEI 49	467.84	Effinger Schichten	80	1928	254	278.5
WEI 50	476.09	Effinger Schichten	92	1224	345	816.9
WEI 1	484.14	Varians-Schichten	156	4015	194	n.d.
WEI 2	495.46	Württembergica-Schichten	130	4215	217	n.d.
WEI 3	506.08	Württembergica-Schichten	113	3663	102	n.d.
WEI 4	517.10	Württembergica-Schichten	162	5829	56	n.d.
WEI 5	527.86	Parkinsoni-Schichten	85	3612	56	n.d.
WEI 6	539.26	Sowerbyi-Sauzei-Schichten	136	5378	120	n.d.
WEI 7	549.62	Murchisonae-Schichten	150	2411	159	n.d.
WEI 51	560.48	Opalinuston	67	1539	266	30.2
WEI 8	561.08	Opalinuston	n.d.	n.d.	n.d.	n.d.
WEI 9	572.80	Opalinuston	109	3623	183	n.d.
WEI 52	581.86	Opalinuston	80	2045	240	5.1
WEI 10	582.04	Opalinuston	n.d.	n.d.	n.d.	n.d.
WEI 11	594.74	Opalinuston	111	898	208	n.d.
WEI 12	605.34	Opalinuston	112	845	306	n.d.
WEI 13	616.32	Opalinuston	111	1110	233	n.d.
WEI 14	627.09	Opalinuston	112	1577	281	n.d.
WEI 15	638.09	Opalinuston	119	881	314	n.d.
WEI 16	649.46	Opalinuston	n.d.	n.d.	n.d.	n.d.
WEI 53	652.20	Opalinuston	115	1909	293	8.5
WEI 17	660.30	Opalinuston	110	1580	207	n.d.
WEI 18	671.89	Posidonienschiefer	106	2943	79	n.d.
WEI 19	682.16	Obtusus-Ton	112	841	166	n.d.
WEI 20	693.19	Obtusus-Ton	101	2488	110	n.d.
WEI 21	703.88	Insektenmergel	172	3918	182	n.d.
WEI 22	715.56	Knollenmergel	148	409	225	n.d.
WEI 54	723.98	Obere Bunte Mergel	144	526	571	88.4
WEI 55	736.12	Schilfsandstein	186	2015	456	26.6
WEI 56	744.63	Gipskeuper	125	1932	445	1.6
WEI 57	757.94	Gipskeuper	76	2015	234	3.1
WEI 58	769.10	Gipskeuper	28	1909	<91	<0.4
WEI 59	782.38	Gipskeuper	51	2009	209	<0.4
WEI 60	790.71	Gipskeuper	87	1806	245	<0.4
WEI 61	802.29	Gipskeuper	113	1966	680	<0.4
WEI 62	812.25	Gipskeuper	83	1814	411	3.1
WEI 63	818.50	Lettenkohle	25	295	<91	1.1

Fig. 6 shows the Br^- concentrations plotted against the Cl^- contents in aqueous leachates, together with the sea-water dilution line (Bruland & Lohan 2003). The following observations can be made:

- Samples from Schafisheim are roughly aligned along the sea-water dilution line, but some samples with unusually high Br^- concentrations in the Keuper are also identified.
- In contrast, several samples from Benken (in particular from the "Brauner Dogger") lie on the low-Br^- side, with Br^- contents frequently below detection.
- Samples from Weiach appear to be occupy an intermediate position between these two trends. The Malm and Keuper samples scatter around the sea-water dilution line, whereas those from the Dogger are relatively depleted in Br^-.
- It is difficult to recognise a trend for Riniken, as the variability in both anions is small. Nevertheless, all samples lie on or below the sea-water dilution line, and some Br^- values are below detection limit.

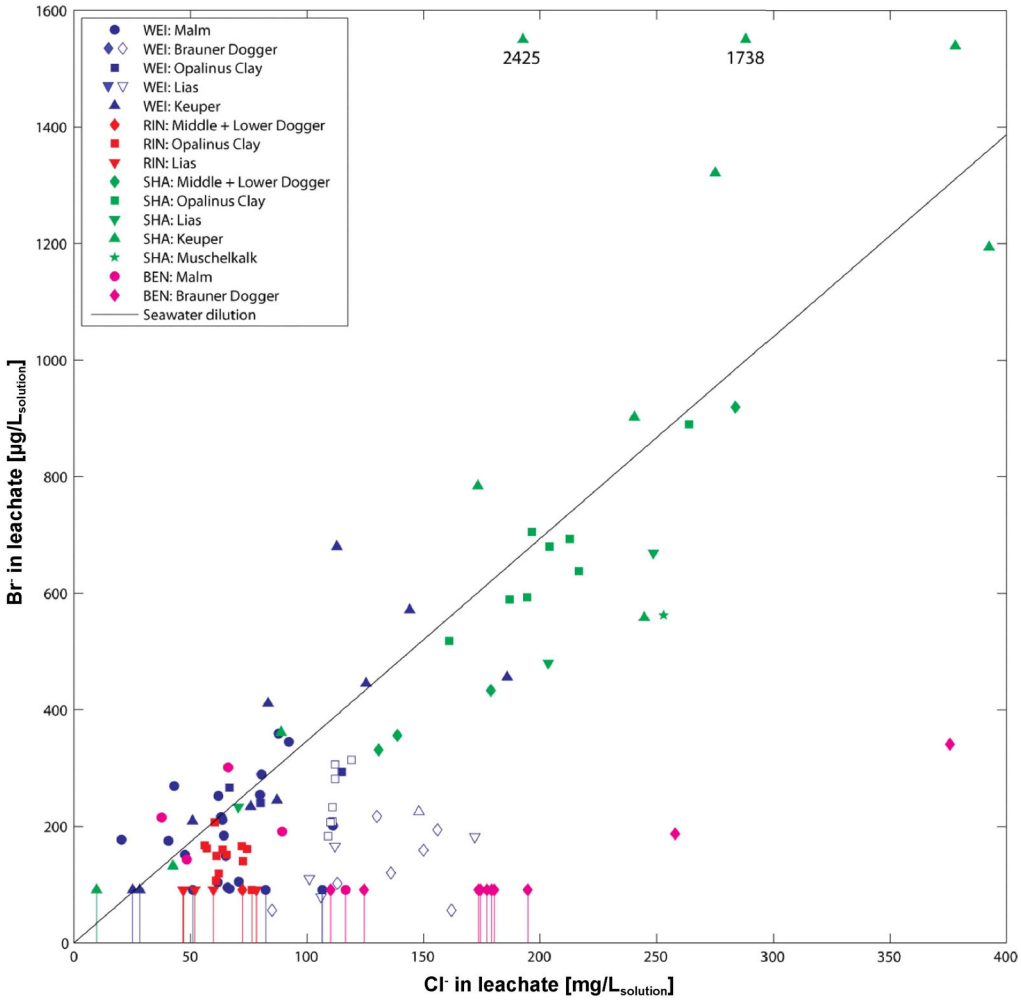

Fig. 6: Cl^- vs. Br^- contents in aqueous leachates

Two outliers are marked with their Br^- values. The sea-water ratio according to Bruland & Lohan (2003) is indicated by the black line. Vertical coloured lines: Values below detection limit, symbol is at the limit. Open symbols in Weiach refer to data produced previously by H. N. Waber

5 Derivation of pore-water concentrations of anions: Analysis of methodological approaches based on data from the Benken borehole

5.1 Formalism

The conversion of the aqueous-leaching data from concentrations per L of leach solution to pore-water concentrations is performed according to

$$C_{pw}\left[\frac{mg}{L_{pore\ water}}\right]=\frac{C_{AqEx}\left[\frac{mg}{L_{solution}}\right]\ \frac{L\left[L_{solution}\right]}{S\left[kg_{dry\ rock}\right]}\rho_g\left[\frac{kg_{dry\ rock}}{L_{rock}}\right](1-n)}{n\ \alpha}$$

with C_{pw} = concentration of solute in pore water
C_{AqEx} = concentration of solute in aqueous extract
L/S = liquid/solid ratio in aqueous-leaching experiments
ρ_g = grain density
n = physical porosity
α = fraction of physical porosity accessible to the solute.

This equation requires knowledge of both physical and of anion-accessible porosity. Given the fact that the samples studied here are at least 10 years old, the determination of porosities is more uncertain than in the situation when the samples are fresh and saturated.

5.2 Methods to constrain physical porosity

Physical porosity for the Benken samples was estimated by three independent methods. These, together with their inherent uncertainties, are listed in Tab. 24.

Tab. 24: Methods to constrain physical porosity in the present study

Method	Uncertainties
1. Porosity calculated from measured bulk dry and grain densities	Possibly limited representativity of measured densities (in particular bulk dry density) for the original *in-situ* conditions: • Samples were exposed to variable temperature and air humidity over many years, with possible effects on pore structure • Oxidation reactions, *e.g.* the conversion of pyrite to gypsum
2. Porosity calculated from RHOB density borehole log	• Vertical resolution of the log is in the range of several dm and so not necessarily sample-specific (average sample length is 22 cm) • Quality of RHOB log strongly depends on borehole quality; no data (or interpolated data) are available in zones with breakouts; logs need to be edited using the caliper log. Breakouts lower RHOB density and so yield an overestimation of porosity • The calculation of porosity requires knowledge of grain density, which has to be constrained by other methods (laboratory measurements on cores or calculation based on mineralogical composition using generic mineral densities)
3. Porosity calculated from clay-mineral content	In clay-carbonate mixtures, a site- or region-specific correlation may be defined. In this study, the following constraints apply: • The number of data that can be used for the correlation is limited, even if the whole Jurassic sequence is considered (the Triassic is excluded because of the occurrence of a wider lithological spectrum (sandstones, evaporites)) • The correlation is not well defined, correlation factors are low • Porosity depends not only on clay-mineral content but also on maximum burial depth, which varies over the region

5. 3 Approaches to defining the anion-accessible porosity fraction

In Opalinus Clay, about half of the physical porosity is accessible to anions (Gimmi & Waber 2004, Pearson *et al.* 2003, Koroleva *et al.* 2011). However, the low-permeability sequence is lithologically heterogeneous, so it is questionable whether the value for Opalinus Clay is representative of the whole profile. The following alternatives were chosen and are illustrated in Fig. 7:

1. The whole physical porosity was assumed to be anion-accessible, *i.e.* all solute concentrations in leachates were directly related to physical porosity;
2. In line with Gimmi & Waber (2004), the anion-accessible porosity fraction was chosen as 0.5 for the whole sequences, irrespective of mineralogy. A cutoff was selected at 10 % clay-mineral content (limestones), at and below which the whole physical porosity was considered to be anion-accessible;
3. A hypothetic function was chosen that considers an anion-accessible porosity fraction of 0.5 in claystones (≥60 % clay-mineral content) and a linear increase towards 1 with decreasing clay-mineral content.

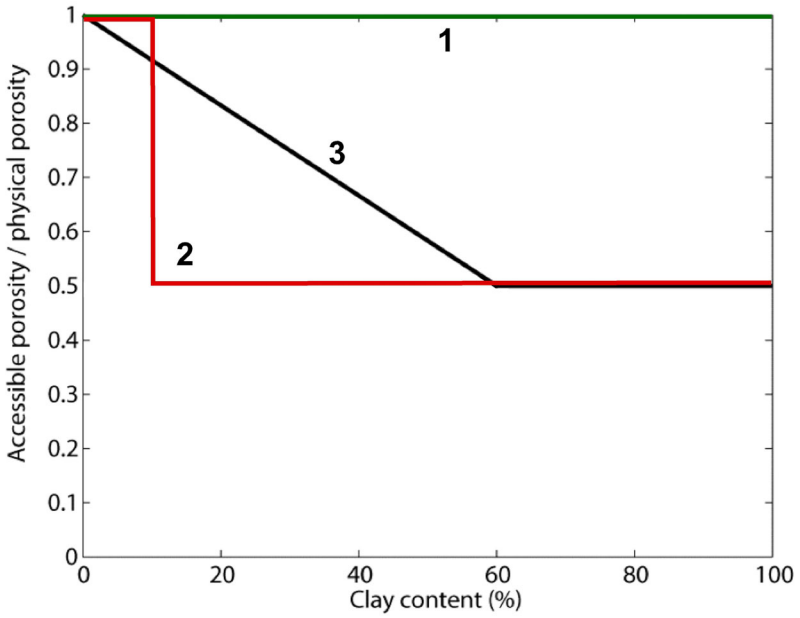

Fig. 7: Hypotheses relating the anion-accessible porosity fraction to clay-mineral content

5.4 Analysis of methods to derive physical and anion-accessible porosity

The approaches presented in Sections 5.2 and 5.3 are explored here using the information from the Benken borehole. This choice was made because abundant data are available from this site (mineralogy, porosity: Nagra 2001, Waber *et al.* 2003, this study; anion contents: Waber *et al.* 2003, this study).

5.4.1 Porosity calculated from measured bulk dry and grain densities and from gravimetric water loss

Porosity data calculated from density measurements and from gravimetric water loss of saturated samples are known to yield comparable results (see, *e.g.*, Nagra 2002), and so are treated together here. Three data sets are available (Tab. 25, Fig. 8):

1. Densities and calculated physical porosity based on this study, *i.e.* performed on 10 years old materials (focussed on samples from the "Brauner Dogger", see also Tab. 16). Uncertainties related to the age of the samples are listed in Tab. 24.
2. Water-loss porosity data from Waber *et al.* (2003) obtained from gravimetric water contents of freshly drilled core material.
3. Densities and calculated physical porosity based on Nagra (2001). The data were produced shortly after drilling and so are not affected by artefacts due to long-term storage. On the other hand, they were obtained by different methods than those for this study.

Tab. 25: Comparison of porosities of Benken drillcores (Jurassic section) derived from different methods

Upper part: Physical porosity obtained from density measurements in this study, ***i.e.*** based on 10 years old core materials, compared with alternative methods to constrain porosity. *Central part:* Porosity obtained from water-loss measurements of the freshly drilled core (Waber ***et al.*** 2003), compared with alternative methods to constrain porosity. *Bottom part:* Physical porosity obtained from density measurements by Nagra (2001), based on fresh core materials, compared with alternative methods to constrain porosity. One low-porosity sample from the Jurensis-Mergel is excluded from the comparison because of the large analytical error

Depth [m]	Formation	Clay-mineral content [wt.-%]	Physical porosity [%]	Water-loss porosity [%]	Porosity from RHOB log [%]	Error rel. to water-loss or phys. por. [rel.%]	Por. based on correlation with clay-mineral content [%]	Error rel. to water-loss or phys. por. [rel.%]
		This study						
395.97	Wohlgeschichtete Kalke	1	3.3				4.1	24.2
407.38	Wohlgeschichtete Kalke	1	3.9		2.5	-35.9	4.2	7.7
417.83	Hornbuck-Schichten	9	4.2		3.5	-16.7	5.3	26.2
428.11	Hornbuck-Schichten	36	9.5		5.8	-38.9	9.7	2.1
443.83	Effinger Schichten	13	8.8		5.9	-33.0	6.1	-30.7
459.90	Varians-Schichten	53	11.9		11.4	-4.2	12.3	3.4
467.12	Parkinsoni-Württemb.-Sch.	51	12.7		10.9	-14.2	12.0	-5.5
476.14	Parkinsoni-Württemb.-Sch.	24	5.8		10.0	72.4	7.8	34.5
481.11	Parkinsoni-Württemb.-Sch.	57	13.1		12.0	-8.4	12.9	-1.5
482.00	Parkinsoni-Württemb.-Sch.	42	11.9		9.5	-20.2	10.6	-10.9
489.15	Parkinsoni-Württemb.-Sch.	52	12.2		11.8	-3.3	12.2	0.0
498.61	Subfurcaten-Schichten	34	14.3		9.1	-36.4	9.3	-35.0
504.45	Subfurcaten-Schichten	36	12.4		12.3	-0.8	9.7	-21.8
507.87	Wedelsandstein-Formation	50	14.1		21.7	53.9	12.0	-14.9
525.45	Wedelsandstein-Formation	14	11.7		10.0	-14.5	6.2	-47.0
525.88	Wedelsandstein-Formation	10	8.1		6.9	-14.8	5.5	-32.1
535.49	Wedelsandstein-Formation	29	9.8		9.9	1.0	8.5	-13.3
		Waber *et al.* (2003)			This study			
439.56	Effinger Schichten	40		13.8	7.6	-44.7	10.3	-25.5
454.95	Varians-Schichten	20		11.5	6.8	-40.8	7.1	-38.1
471.49	Parkinsoni-Württemb.-Sch.	54		12.4	13.1	+5.3	12.5	+1.0
485.50	Parkinsoni-Württemb.-Sch.	45		10.8	10.6	-2.0	11.1	+2.3
502.45	Blagdeni-Schichten			12.2	12.0	-1.9		
514.25	Wedelsandstein-Formation	42		11.6	9.0	-23.1	10.6	-8.8
545.16	Achdorf-Formation	57		12.6	9.8	-22.1	13.0	+3.4
563.85	Opalinuston	52		11.7			12.2	+4.6
571.55	Opalinuston	23		5.3	5.2	-2.9	7.6	+42.5
593.85	Opalinuston			10.7	8.8	-18.2		
613.48	Opalinuston	56		12.5	10.4	-17.0	12.8	+2.4
645.05	Opalinuston	62		12.3	8.8	-28.1	13.8	+12.3
645.65	Opalinuston	66		11.1	8.9	-19.8	14.4	+30.4
657.35	Jurensis-Mergel			9.7	5.2	-45.8		
663.85	Posidonienschiefer	42		10.8	18.6	73.0	10.6	-1.5
674.11	Obtusus-Ton			10.7	9.3	-13.0		
683.27	Obtusus-Ton	67		9.0	7.1	-21.0	14.6	+62.4
		Nagra (2001)			This study			
401.68	Wohlgeschichtete Kalke	3	3.4		2.9	-13.4	4.4	+31.3
454.95	Varians-Schichten	20	9.9		6.8	-31.0	7.1	-28.6
519.96	Wedelsandstein-Formation	6	9.1		7.3	-19.0	4.9	-45.4
545.16	Achdorf-Formation	57	11.3		9.8	-13.6	12.9	+14.1
555.31	Achdorf-Formation	62	10.4		10.8	+3.5	13.9	+33.4
571.55	Opalinuston	23	7.4		5.2	-30.3	7.6	+2.1
576.90	Opalinuston		11.5		5.9	-48.5		
582.09	Opalinuston	52	8.8		9.1	+3.4	12.2	+39.3
586.61	Opalinuston		10.8		9.2	-15.1		
601.04	Opalinuston		13.1		12.9	-1.4		
613.48	Opalinuston	55	12.5		10.4	-16.6	12.7	+2.3
637.01	Opalinuston	67	10.0		8.7	-13.1	14.6	+45.5
645.05	Opalinuston	62	12.4		8.8	-28.6	13.9	+12.2
678.26	Obtusus-Ton		13.4		9.5	-28.7		
683.27	Obtusus-Ton	66	13.2		7.1	-46.4	14.4	+8.6

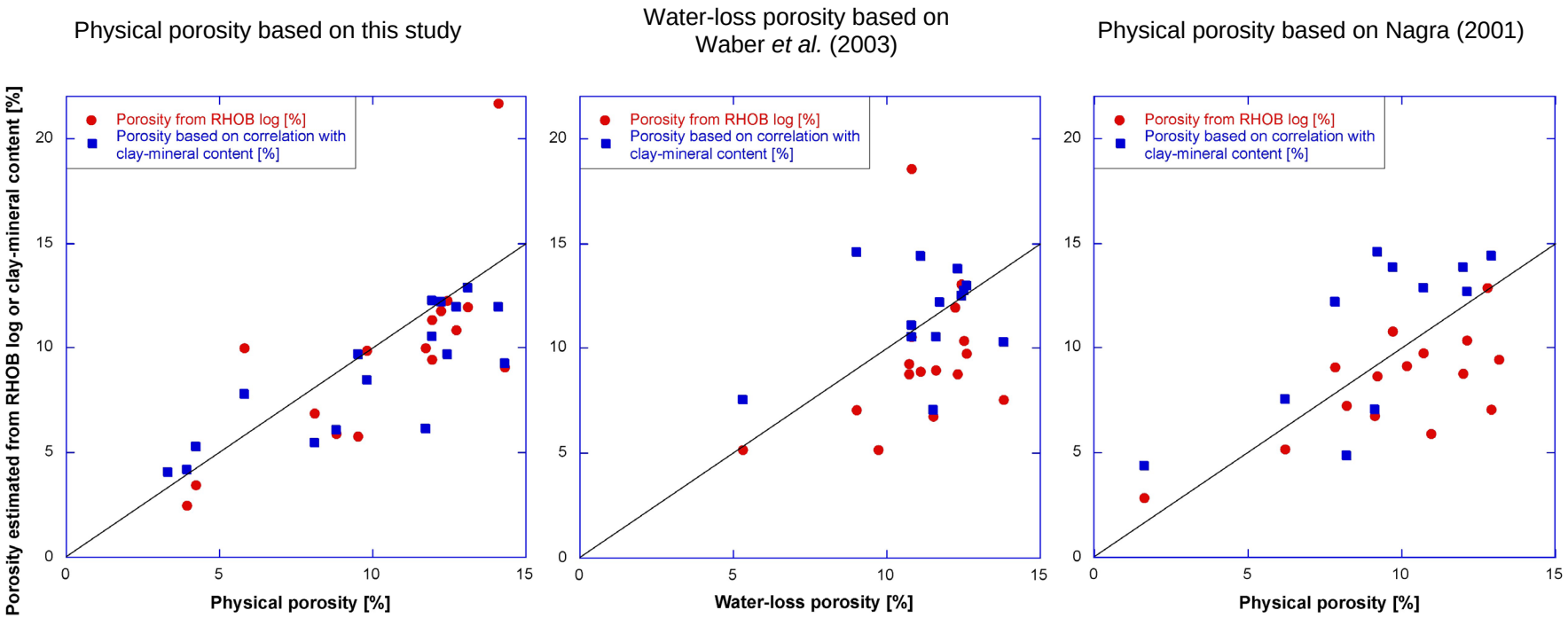

Fig. 8: Comparison of porosities of Benken drillcores (Jurassic section) derived from different methods (based on data from Tab. 25)

Black lines indicate 1:1 correlations. *Left:* Physical porosity obtained from density measurements in this study, *i.e.* based on 10 years old core materials, compared with alternative methods to constrain porosity. *Centre:* Porosity obtained from water-loss measurements of the freshly drilled core (Waber *et al.* 2003), compared with alternative methods to constrain porosity. *Right:* Physical porosity obtained from density measurements by Nagra (2001), based on fresh core materials, compared with alternative methods to constrain porosity. One low-porosity sample from the Jurensis-Mergel is excluded from the comparison because of the large analytical error

5.4.2 Porosity calculated from RHOB density log

A quality-assured RHOB log (ρ_{RHOB}) for the Benken borehole is available in Nagra (2001). The grain densities were derived from mineral-specific values (calcite: 2.71 g/cm^3, dolomite: 2.845 g/cm^3, clay minerals: 2.64 g/cm^3, quartz: 2.625 g/cm^3, anhydrite: 2.97 g/cm^3, pyrite: 5.01 g/cm^3) and from the mineralogical log from Nagra (2001), which provides a continuous depth profile for the contents of clay minerals, carbonates, anhydrite and quartz. In the Jurassic section, carbonate was assumed to be pure calcite, and all samples were assumed to contain 0.5 wt.-% pyrite. In the Triassic, a dolomite/calcite ratio of 3 was used, and no pyrite was considered. Porosity was calculated according to

$$n = \frac{\rho_g - \rho_{RHOB}}{\rho_g - \rho_{fluid}} \quad ,$$

with ρ_{fluid} = fluid density = 1 g/cm^3. The resulting data are listed in Tab. 25.

5.4.3 Porosity calculated from clay-mineral content

In order to establish an empirical relationship between clay-mineral content and physical porosity, only Jurassic samples from this study were used. Jurassic lithologies can be roughly conceived as mixtures of clay minerals and calcite in variable proportions, whereas the lithological spectrum is more complex in the Triassic (including sandstones, evaporites, dolomitic rocks). In addition to data from Benken, those from Weiach were also included in the analysis, in order to augment the data base. This is justified because the burial histories of Benken and Weiach are similar, whereas those of the other studied boreholes are different (Mazurek *et al.* 2006) and so may lead to different porosities at a given clay-mineral content. The resulting correlation is shown in Fig. 9a. The regression is not overly well defined, the scatter of the data is considerable. Porosities derived from the regression of clay-mineral contents (black line in Fig. 9a) are given in Tab. 25.

Further data on clay-mineral contents and porosities from Benken and Weiach are available from the original reports prepared in the context of the respective drilling campaigns (Nagra 2001, Matter *et al.* 1988a; data compiled in Mazurek 2011). The advantage of these data is the fact that the analyses were made shortly after core recovery, so effects of oxidation and long-term storage are expected to be less important. However, the data, as illustrated in Fig. 9b, show a more substantial scatter than those obtained in the frame of this study (Fig. 9a), and a meaningful regression of porosities to clay-mineral contents cannot be obtained. The reasons for the scatter are not entirely clear. It must be noted that the methodology used to measure densities that underlie the porosities of Fig. 9b was different from that used here.

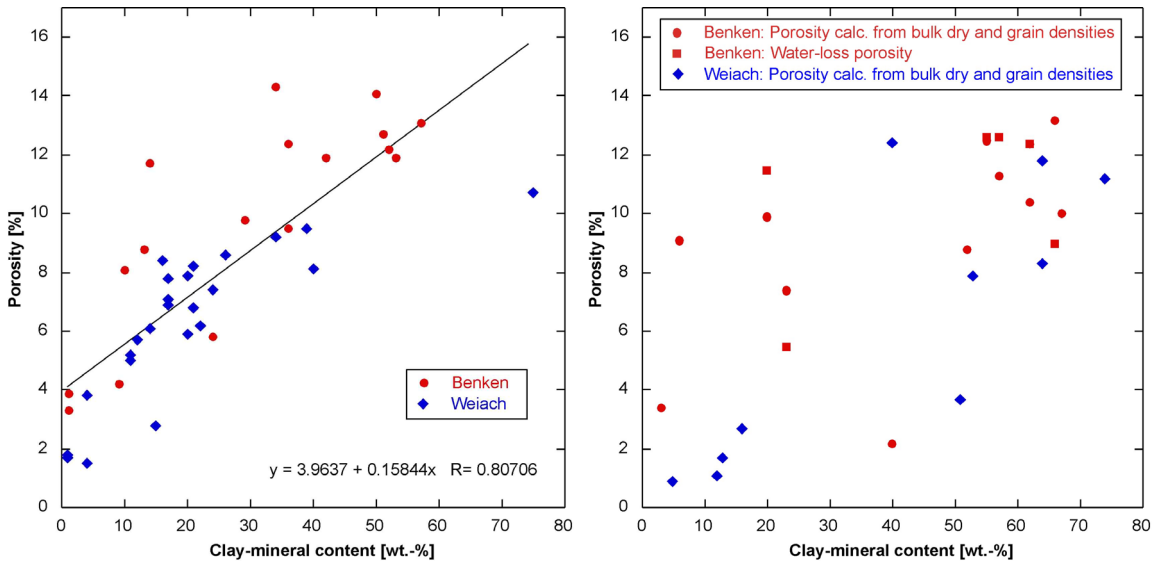

a. b.

Fig. 9: Correlation of clay-mineral contents and porosities of the Jurassic sections in boreholes Benken and Weiach

a. Data from this study

b. Data from Nagra (2001) and Matter *et al.* (1988a)

5.4.4 Evaluation of methods to constrain porosity

Because the true porosity values are not known and each method has its own uncertainties (see Tab. 24), it is not possible to evaluate the adequacy of the individual data sets against an accepted benchmark. Porosities estimated from the RHOB log and from clay-mineral content show deviations from physical or water-loss porosity of up to 73 % relative. The average relative errors are ±20 - 25 % for both RHOB-derived porosities and for porosities estimated from clay-mineral contents (Tab. 25).

Because a clearly preferred method to characterise porosity of "historic" samples has not been identified, they were all considered here in alternative cases for the derivation of pore-water concentrations of solutes according to the equation given in Section 5.1. Together with the 3 alternative ways to take into account anion exclusion (Section 5.3, Fig. 7), a total of 9 cases were explored. The resulting pore-water concentrations of Cl^- are listed in Tab. 26 and plotted in Fig. 10 - 12.

Given the fact that the pore-water profile in Benken is considered to be dominated by diffusion (Gimmi & Waber 2004, Gimmi *et al.* 2007), a regular pattern of the spatial Cl^- distribution would be expected. Therefore, recalculation methods that yield regular patterns are considered as more appropriate, whereas scattered distributions are thought to be more strongly affected by artefacts or inadequate assumptions. In this respect, inspection of Fig. 10 - 12 leads to the following insights:

- In Fig. 10, the data of Waber *et al.* (2003) (shown in blue) yield a regular pattern when using the original water-loss porosities for the recalculation (left). An almost equally regular pattern is obtained when using porosities derived from the correlation with clay-mineral contents (right). In contrast, the pattern obtained when using porosities derived from the RHOB log is scattered and probably not representative.

- In the same Figure, the data produced in this study (red) are substantially more strongly scattered than those of Waber *et al.* (2003), which reflects the larger uncertainties regarding porosity. Remarkably, the distribution is most regular when using porosities derived from clay-mineral contents (right), even though 3 points fall off the general trend (for a discussion of these data, see screening of the results in Section 6.2). In any case, this data set appears to be better interpretable than the other two.
- Fig. 11, in which the same data are shown but where, in addition, a scaling for the anion-accessible porosity fraction was applied (factor 0.5 for samples with clay-mineral contents >10 wt.-%), yields similar conclusions. The central graph based on RHOB data is quite scattered, whereas the other two show clearer trends (in spite of some outliers in the data set produced in this study). The Cl^- concentration in the shallowest sample is reasonably close to that of the overlying Malm aquifer (4356 mg/L at a depth of 380 - 394.8 m; see Tab. 2).
- In the graphs shown in Fig. 12, anion exclusion is considered using a scaling factor that depends on clay-mineral content (Section 5.3). In comparison to the alternatives shown in the previous Figures, the scatter of the data is clearly higher, in particular in those of Waber *et al.* (2003). It appears that a constant scaling factor (except in limestones) better approaches the *in-situ* values.

5.5 Conclusions for the calculation of pore-water concentrations of solutes

Based on the analysis in the previous Section, the following conclusions are made:

- Aqueous-leaching data are ideally recalculated using water-loss porosity of the same samples. In the absence of water-loss porosity data, the second choice is porosity derived by correlation to clay-mineral content. Porosity based on new density measurements on the 10 years old samples is the third choice. Porosity derived from the RHOB log cannot be used, probably due to the more limited spatial resolution of this method and because of possible artefacts, *e.g.* breakouts).
- Regarding the scaling factor that considers anion exclusion in clay-bearing rocks, the variant using a constant factor in conjunction with a cutoff at 10 % clay-mineral content yields more consistent results than a mineralogy-dependent function. It will be used for the calculations in Section 6 below. In the absence of direct experimental data, it is difficult to provide an error estimation for this approach.

Tab. 26: Pore-water chloride contents calculated from aqueous-leaching data of Benken samples using a set of alternative assumptions regarding porosity

The same procedures were applied to the original leaching data (concentrations per L leach solution) from this study and to those from Waber *et al.* (2003)

					No scaling for anion-accessible porosity			Scaling factor 0.5 used for samples with clay contents >10 wt.-%			Scaling factor depending on clay-mineral content		
Depth [m]	Formation	Clay-mineral content [wt.-%]	Physical porosity [%]	Water-loss porosity (105 °C) [%]	Cl^- in pore water using measured physical or water-loss porosity [mg/L]	Cl^- in pore water using porosity from RHOB log[mg/L]	Cl^- in pore water using porosity derived by correlation with clay content [mg/L]	Cl^- in pore water using measured physical or water-loss porosity [mg/L]	Cl^- in pore water using porosity from RHOB log[mg/L]	Cl^- in pore water using porosity derived by correlation with clay content [mg/L]	Cl^- in pore water using measured physical or water-loss porosity [mg/L]	Cl^- in pore water using porosity from RHOB log[mg/L]	Cl^- in pore water using porosity derived by correlation with clay content [mg/L]
Based on data from this study													
395.97	Wohlgeschichtete Kalke	1	3.3		5237		4130	5237		4130	5284		4167
407.38	Wohlgeschichtete Kalke	1	3.9		2533	4041	2397	2533	4041	2397	2560	4084	2422
417.83	Hornbuck-Schichten	9	4.2		3007	3563	2328	3007	3563	2328	3239	3838	2508
428.11	Hornbuck-Schichten	36	9.5		3041	5228	2990	6081	10456	5979	4339	7460	4266
443.83	Effinger Schichten	13	8.8		2567	3899	3821	5134	7797	7643	2885	4381	4294
459.90	Varians-Schichten	53	11.9		3466	3643	3338	6931	7286	6676	6193	6510	5965
467.12	Parkinsoni-Württemb.-Sch.	51	12.7		3247	3865	3447	6494	7730	6894	5647	6722	5995
476.14	Parkinsoni-Württemb.-Sch.	24	5.8		4794	2637	3490	9589	5274	6979	5991	3295	4361
481.11	Parkinsoni-Württemb.-Sch.	57	13.1		3515	3892	3560	7030	7783	7121	6655	7369	6742
482.00	Parkinsoni-Württemb.-Sch.	42	11.9										
489.15	Parkinsoni-Württemb.-Sch.	52	12.2		3489	3644	3494	6977	7289	6988	6171	6446	6180
498.61	Subfurcaten-Schichten	34	14.3		6289	10535	10257	12578	21070	20514	8739	14639	14253
504.45	Subfurcaten-Schichten	36	12.4		4994	5043	6561	9989	10086	13122	7175	7245	9426
507.87	Wedelsandstein-Formation	50	14.1		2931	1734	3547	5861	3469	7094	5055	2991	6118
525.45	Wedelsandstein-Formation	14	11.7										
525.88	Wedelsandstein-Formation	10	8.1		5446	6517	8261	5446	6517	8261	5925	7091	8988
535.49	Wedelsandstein-Formation	29	9.8		3085	3036	3604	6170	6072	7208	4049	3984	4730
Based on data from Waber *et al.* (2003)													
439.56	Effinger Schichten	40		13.8	2465	4774	3442	4930	9548	6884	3697	7161	5163
454.95	Varians-Schichten	20		11.5	1950	3469	3306	3901	6937	6613	2341	4162	3968
471.49	Parkinsoni-Württemb.-Sch.	54		12.4	3244	3058	3209	6488	6116	6418	5898	5560	5834
485.50	Parkinsoni-Württemb.-Sch.	45		10.8	3705	3788	3610	7409	7575	7219	5927	6060	5776
502.45	Blagdeni-Schichten			12.2	3168	3237		6336	6475				
514.25	Wedelsandstein-Formation	42		11.6	3378	4527	3746	6756	9054	7492	5197	6965	5763
545.16	Achdorf-Formation	57		12.6	3383	4480	3256	6765	8961	6512	6443	8534	6202
563.85	Opalinuston	52		11.7	3077		2925	6155		5851	5431		5162
571.55	Opalinuston	23		5.3	3221	3322	2207	6443	6645	4414	3985	4110	2730
593.85	Opalinuston			10.7	3191	3984		6382	7968				
613.48	Opalinuston	56		12.5	2562	3164	2492	5125	6328	4985	4804	5933	4673
645.05	Opalinuston	62		12.3	2379	3440	2083	4758	6881	4165	4758	6881	4165
645.65	Opalinuston	66		11.1	2432	3109	1795	4863	6217	3589	4863	6217	3589
657.35	Jurensis-Mergel			9.7	3040	5881		6080	11762				
663.85	Posidonienschiefer	42		10.8	3004	1584	3056	6009	3168	6112	4622	2437	4701
674.11	Obtusus-Ton			10.7	1378	1609		2756	3219				
683.27	Obtusus-Ton	67		9.0	1546	1999	894	3093	3998	1788	3093	283	1788

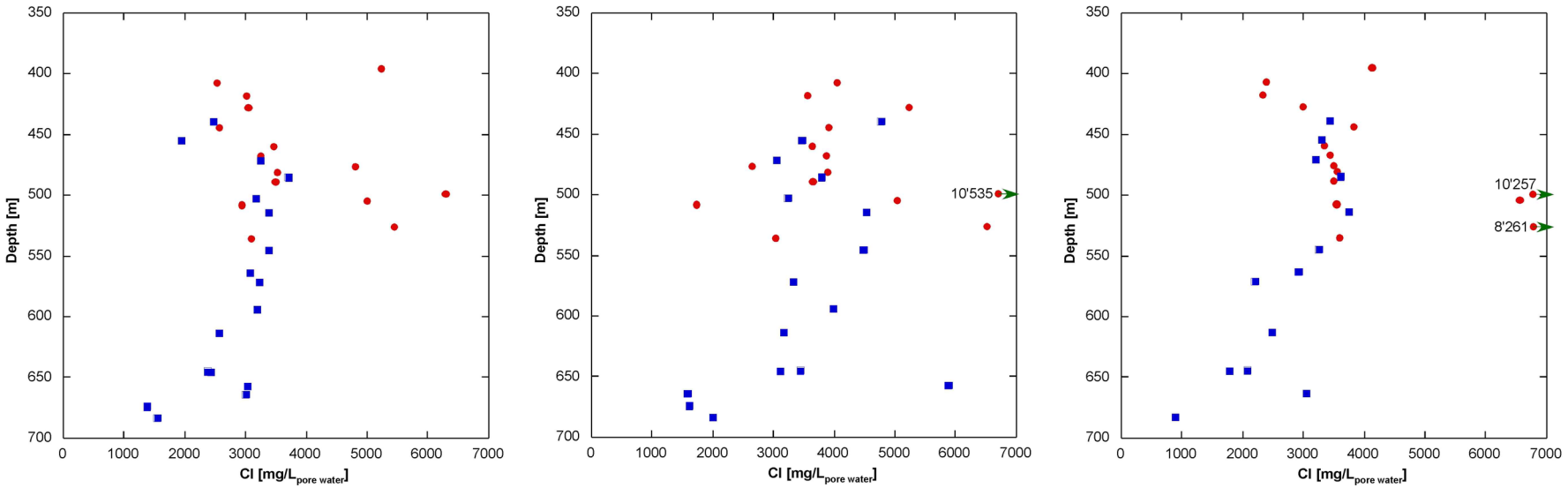

Fig. 10: Chloride contents from aqueous leaching of Benken samples recalculated to pore-water contents without any correction for the anion-accessible porosity fraction

Red: leaching data from this study; blue: leaching data from Waber *et al.* (2003). *Left:* Recalculation based on physical porosity obtained from density measurements (data from this study) or water-loss porosity (data from Waber *et al.* 2003). *Centre:* Recalculation based on porosity obtained from RHOB borehole log. *Right:* Recalculation based on porosity derived from the correlation with clay-mineral contents

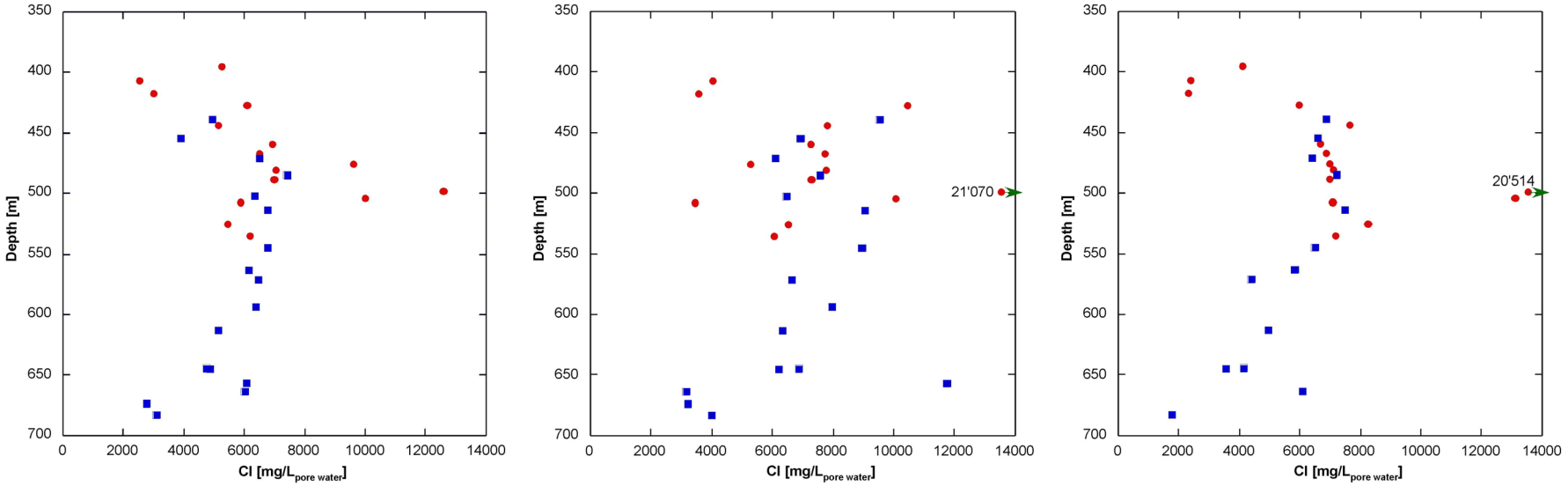

Fig. 11: Chloride contents from aqueous leaching of Benken samples recalculated to pore-water contents, considering a scaling factor of 0.5 for the anion-accessible porosity fraction in samples with >10 wt.-% clay-mineral content

Red: leaching data from this study; blue: leaching data from Waber *et al.* (2003). *Left:* Recalculation based on physical porosity obtained from density measurements (data from this study) or water-loss porosity (data from Waber *et al.* 2003). *Centre:* Recalculation based on porosity obtained from RHOB borehole log. *Right:* Recalculation based on porosity derived from the correlation with clay-mineral contents

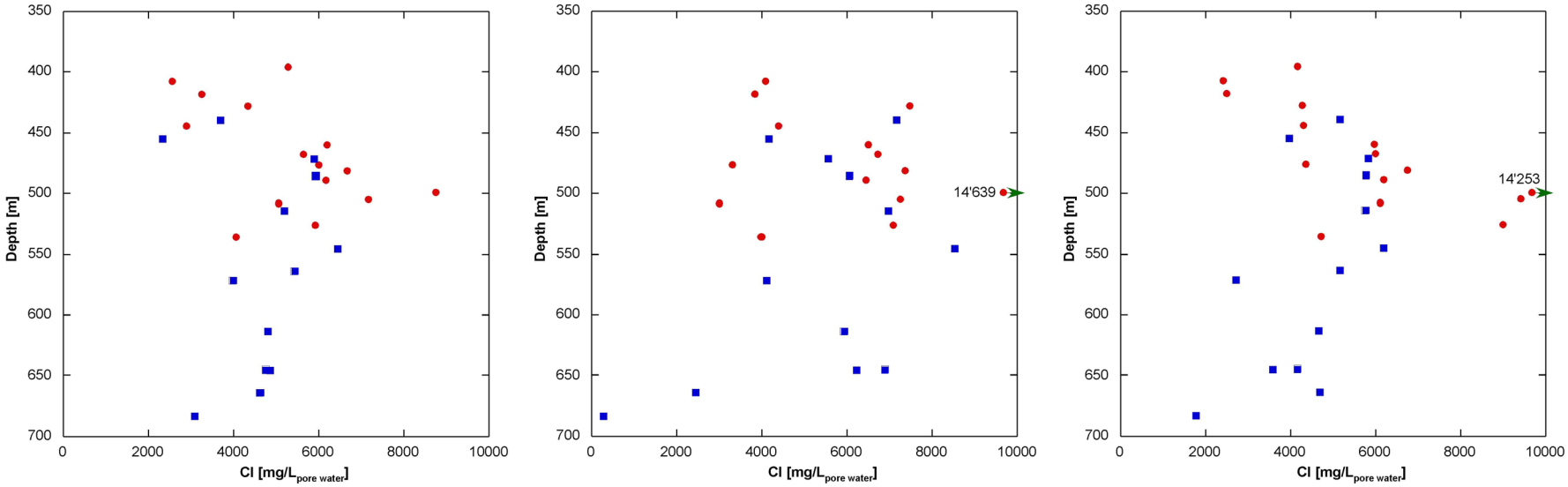

Fig. 12: Chloride contents from aqueous leaching of Benken samples recalculated to pore-water contents, considering a mineralogy-dependent scaling factor for the anion-accessible porosity fraction (see text)

Red: leaching data from this study; blue: leaching data from Waber *et al.* (2003). *Left:* Recalculation based on physical porosity obtained from density measurements (data from this study) or water-loss porosity (data from Waber *et al.* 2003). *Centre:* Recalculation based on porosity obtained from RHOB borehole log. *Right:* Recalculation based on porosity derived from the correlation with clay-mineral contents

6 Calculated pore-water concentrations of Cl^- in all boreholes

6.1 Analysis of errors and error propagation

Pore-water concentrations of solutes are recalculated from concentrations in aqueous extracts (C_{AqEx}) to pore-water concentrations (C_{pw}) using the equation given in Section 5.1. Apart from C_{AqEx}, the parameters in this equation include grain density (ρ_g), porosity (n) (and therefore bulk dry density $\rho_{b,dry}$ that is used to calculate porosity) and the anion-accessible porosity fraction (α). All these parameters are subject to errors and uncertainties, and Tab. 27 provides an overview of these. The total error is dominated by uncertainties regarding porosity and the fraction that is accessible to anions.

6.1.1 Porosity obtained from density measurements

The purely analytical errors on the measurement of bulk dry and grain density are about ±1.2 and 1.3 $\%_{rel.}$, originating mainly from the error on the density of the immersion fluid (paraffin, kerosene) that is used to calculate the rock density values. These errors correspond to absolute errors of about 0.03 - 0.035 g/cm^3 for both densities. Using the error-propagation function formulated in Section 3.2.3, these errors propagate into an error of around ±1.6 vol.-% on porosity. This error remains essentially constant irrespective of the porosity value. Therefore, the relative error increases with decreasing porosity.

The long-term storage of the core materials under atmospheric conditions is a further potential source of uncertainty that adds up with the analytical error. In order to capture this effect, an additional estimated error of 20 $\%_{rel.}$ was applied on porosity. For a rock with a porosity of 10 %, the total uncertainty of 3.6 vol.-% (considering both the analytical and the sample storage uncertainties) corresponds to a relative error of ±36 $\%_{rel.}$. For a rock with a porosity of 5 %, the relative error becomes ±52 $\%_{rel.}$.

6.1.2 Porosity obtained by regression to clay-mineral content

A linear correlation was established between clay-mineral content and physical porosity for Jurassic samples from the Benken and Weiach boreholes analysed in this study (Section 5.4.3, Fig. 9a). Porosity values calculated from known clay-mineral contents were then compared with porosities derived from water-loss and density measurements on fresh samples from Benken (Tab. 25). This comparison indicated that 68 % of the calculated porosities are within ±30 $\%_{rel.}$ of the values based on density and water-loss measurement. Therefore, an estimated error of ±30 $\%_{rel.}$ is propagated into the calculation of solute concentrations in pore water.

The regression line obtained for samples from Benken and Weiach is also used below for the other boreholes. This adds another element of uncertainty because the burial histories of these boreholes differ somewhat from that of the Benken/Weiach region (Mazurek *et al.* 2006). In principle, the relationship between clay-mineral content and porosity should be elaborated for each borehole, but this is not feasible in this case due to the limited data available from boreholes Riniken and Schafisheim.

Tab. 27: Definition and quantification of errors of parameters that are used to calculate pore-water concentrations of solutes

Parameter	Symbol	Source of error	Quantification of error	Further sources of error not included in the quantification
Solute concentration in aqueous extract	C_{AqEx}	Analytical error of IC or ICP-MS analysis	±5 $\%_{rel.}$ for Cl^-, ±15 $\%_{rel.}$ for Br^- and I^-	
Grain density	r_g	Analytical error, dominated by the error on kerosene density (±0.01 g/cm^3)	±1.3 $\%_{rel.}$	Sample heterogeneity
Bulk dry density	$r_{b,dry}$	Analytical error, dominated by the error on paraffin density (±0.01 g/cm^3)	±1.2 $\%_{rel.}$	• Sample heterogeneity • Textural and mineralogical changes due to long-term storage of core materials under atmospheric conditions • Possible shrinkage of clay-rich samples due to drying (for a discussion of this effect see Mazurek *et al.* 2010)
Physical porosity (obtained from density measurements)	n	Analytical error on density measurements	Calculated from errors on $r_{b,dry}$ and r_g: yields *ca.* ±1.6 vol.-%, independently of the value of porosity	• Sample heterogeneity • Possible shrinkage of clay-rich samples due to drying (for a discussion of this effect see Mazurek *et al.* 2010)
		Effects of textural and mineralogical changes due to long-term storage of core materials under atmospheric conditions on $r_{b,dry}$	±20 $\%_{rel.}$ of the porosity value (estimate)	
Porosity obtained by regression to clay-mineral content	n	Definition of the regression line	±30 $\%_{rel.}$ (based on comparison with porosities obtained from water-loss and density measurements, see Tab. 25)	Extrapolation of the regression developed for Benken and Weiach to the other boreholes
Anion-accessible porosity fraction	a	Conceptual assumption on the fraction of physical porosity accessible to anions	Not quantified	

6.1.3 Calculation of total errors

The propagated error on the calculated concentrations is quantified using the Gaussian law of uncertainty propagation applied to the equation given in Section 5.1. The rock/water ratio L/S [$L_{solution}/kg_{dry\ rock}$] of the experiments was 1, so this term drops out from the equation. The partial derivatives that propagate the errors (u) on the concentration in the extract (C_{AqEx}), grain density (ρ_g) and porosity (n) are

$$\frac{\partial C_{pw}}{\partial C_{AqEx}} = \frac{(1-n)\cdot\rho_g}{n\cdot\alpha}$$

$$\frac{\partial C_{pw}}{\partial \rho_g} = C_{AqEx}\frac{(1-n)}{n\cdot\alpha}$$

$$\frac{\partial C_{pw}}{\partial n} = -C_{AqEx}\frac{\rho_g}{n^2\cdot\alpha},$$

leading to a total uncertainty on the pore-water concentration of

$$u_{C_{pw}} = \frac{1}{n\cdot\alpha}\sqrt{\left((1-n)\cdot\rho_g\cdot u_{C_{AqEx}}\right)^2 + \left((1-n)\cdot C_{AqEx}\cdot u_{\rho_g}\right)^2 + \left(\frac{C_{AqEx}\cdot\rho_g\cdot u_n}{n}\right)^2}.$$

Note that the error on the fraction of porosity that is accessible to anions (α, see Section 5.3) cannot be quantified because it relies on conceptual assumptions that cannot currently be rigorously tested against experimental data.

6.2 Calculated Cl^- concentrations in pore water and data screening

The resulting pore-water concentrations of Cl^-, including the propagated errors according to Tab. 27, are listed in Tab. 28 - 31 for boreholes Benken, Riniken, Schafisheim and Weiach. Results are shown both for concentrations recalculated using physical porosity based on density measurements in this study and for those recalculated using the regression to clay-mineral contents. The anion-accessible porosity fraction α was assumed to be 0.5 for rocks with >10 wt.-% clay-mineral content and 1 for ≤10 wt.-% clay-mineral content. Graphical representations of the results are shown in Fig. 13 - 20.

The spatial distributions of Cl^- do show depth trends. Interestingly, clearer and more consistent depth profiles are obtained when the recalculation of the concentrations is based on porosities obtained from the regression to clay-mineral contents. Nevertheless, there are a number of outliers that do not fit the patterns, and an attempt was made to explain these:

- Some of the outliers are likely due to the somewhat artificial choice of the limit at 10 wt.-% clay-mineral content at and below which the anion-accessible porosity fraction α is assumed to be 1 (see *e.g.* 4 samples between 300 and 400 m in Weiach, Fig. 20).
- A source of error that is not considered by the error bars is sample heterogeneity on the scale of centimetres. Homogeneity was one of the first-order criteria to select core samples for this study. Nevertheless, marked heterogeneity was identified in some samples, in particular in the Keuper. If the sample materials on which porosity, mineralogy and Cl^- contents per kg rock were analysed differ, an additional error applies on the calculated pore-water concentrations of Cl^-. The variability of individual bulk-dry density analyses, each performed on adjacent but not identical pieces of the sample, is taken here as a measure of small-scale heterogeneity. In Tab. 16 - 19, the density data are expressed as averages of all individual measurements on a sample, and heterogeneity is expressed as the standard deviation of all measurements. If the latter exceeds 0.03 g/cm^3, the effect on pore-water concentrations of Cl^- is considered to be substantial (but is not captured by the error bars). Many of the heterogeneous samples are from the Keuper.
- Porosity data for low-porosity rocks are more uncertain than those for rocks with higher porosities. While this effect is included in the estimation of the errors of the calculated

pore-water concentrations of Cl^-, samples with a physical porosity <5 % are highly sensitive to all kinds of errors, not all of which may have been accounted for properly.

Data points to which one or more of these screening criteria apply are highlighted by different symbols in Fig. 13 - 20. Indeed, a large part of the outliers corresponds to such samples, and the spatial Cl^- concentration patterns become clearer if they are suppressed.

6.3 Conclusions

Fig. 21 - 24 show the screened profiles based on porosity derived from clay-mineral contents, together with polynomial fits that indicate the general trends of the data. Only the screened data points, plus the values of the adjacent ground-water samples, were used to calculate these fits. The following conclusions can be drawn from these Figures:

- As shown in Fig. 21, the new data obtained in the "Brauner Dogger" and Malm of Benken fit well together with those of Waber *et al.* (2003). Due to the large error bars and due to the fact that no reliable data could be produced in the uppermost part of the profile (low-porosity limestones), the new data no not contribute substantially to a better definition of the profile as known from the older work.
- The Riniken profile is reasonably well defined in Opalinus Clay but scatters in the Lias (Fig. 22). Due to this and due to the fact that the upper two thirds of the low-permeability sequence cannot be characterised (no core), the data are not suited for quantitative evaluation. The regression line in Fig. 22 suggests a curved profile. However, a straight line corresponding to the Cl^- concentration of the Keuper aquifer would also be consistent with most data points within error.
- Cl^- contents in the Schafisheim profile (up to 15'000 mg/L) are higher than at the other sites (Fig. 23). The scatter is acceptable in Opalinus Clay but is substantial in the Lias and Keuper. Again, the upper part of the profile cannot be characterised (no core).
- The Weiach profile shows well defined depth trends (Fig. 24). The ground-water sample taken in the Malm fits well with the pore-water data from the underlying units. Cl^- contents increase with depth and then remain at 5000 - 6000 mg/L down to the basis of the Malm. There is a marked depression of Cl^- contents in the Dogger (≤4000 mg/L in Opalinus Clay), followed by higher values in the Lias and Keuper (note that this depression is less well expressed when considering the data recalculated using physical porosity; see Fig. 19). There are no reliable data from the lower part of the Keuper, but the Cl^- contents must decrease sharply in order to reach the low value of the Muschelkalk ground water. The steepness of the profile in this lowermost part tends to suggest that either the freshening within the Muschelkalk aquifer is a geologically young feature, or that diffusion coefficients are very low in the lower Keuper. Some constraints on the times involved could be obtained by transport modelling.
- The high Cl^- contents in the upper Keuper of Weiach contrast with the low values at Benken, which are due to the existence of the aquifer horizon in the Sandsteinkeuper. This aquifer does not exist in Weiach.
- The Cl^- profile at Benken indicates that salinity is highest in the centre of the low-permeability sequence and decreases towards the boundaries (in particular towards the underlying Keuper). This suggests that the salinity of the embedding aquifers decreased over time, leading to a diffusive loss of Cl^- from the low-permeability sequence (Gimmi *et al.* 2007). The trends in the other three boreholes are less clear, mainly due to the substantial total errors (Fig. 22 - 24). Nevertheless, in Weiach, it appears that Cl^- content in Opalinus Clay tends to be slightly lower than in the outer parts of the low-permeability sequence. This is either an artefact (*e.g.* related to a possible spatial variability of the Cl^- -

accessible porosity fraction) or a real feature. In the latter case, a complex salinity evolution in the embedding aquifers would have to be considered, with periods of rising salinity. However, given the large errors on the data, this remains hypothetical and cannot be further quantified with confidence.

Regarding the regional distribution of salinity in the potential host-rock units, the following conclusions can be made:

- For the Opalinus Clay and the "Brauner Dogger", Mäder (2009a, Tab. 6-4) derived a reference pore-water concentration for Cl^- of 5672 mg/kg_{H2O}. A high-salinity variant based on leaching data from Mont Russelin (Folded Jura) yielded Cl^- = 23'470 mg/kg_{H2O} (Mäder 2009a, Tab. 6-3). The screened data shown in Fig. 21 - 24 yield the following ranges (rounded to two significant digits): BEN – 3900 to 7600 mg/L; RIN – 2000 to 3400 mg/L; SHA – 5600 to 9600 mg/L; WEI – 3300 to 5900 mg/L. While the high values of the Mont Russelin are not nearly attained in any of the four boreholes, values somewhat below the reference of 5672 mg/kg_{H2O} are identified in three of them.
- It is remarkable that Cl^- content in Opalinus Clay is lowest in the borehole where the formation occurs at relatively shallow level (Riniken – 331 to 451 m) and highest where it is most deeply buried (Schafisheim – 1001 - 1080 m), with Benken and Weiach in intermediate positions both in terms of Cl^- contents and of current burial depth.
- For the Effinger Schichten in the Jura Südfuss area, Mäder (2009b, Tab. 7-8 and 8-1) gave a reference range for Cl^- of 20'000 to 39'000 mg/kg_{H2O}. He also identified major uncertainties in this range, related to the poorly constrained anion-accessible porosity fraction and to limitations in the data base. According to Fig. 21 and Fig. 24, the values of the screened data of this report are 7600 mg/L (Benken) and 4300 - 6600 mg/L (Weiach). These Cl^- concentrations are well below the lower limit given by Mäder (2009b). Ongoing work suggests that the high-salinity variant of the reference water with a Cl^- concentration of 39'000 mg/kg_{H2O} is probably not realistic and based on assumptions that are not considered adequate.

Tab. 28: Calculated pore-water concentrations of Cl^- for the Benken profile

Cl^- (phys. por.) was calculated using porosity obtained from densities; Cl^- (clay-min. cont.) was calculated using porosity derived from clay-mineral content, applying the regression for samples from boreholes Benken and Weiach (Fig. 9). The fraction of anion-accessible porosity was assumed to be 0.5 for rocks with >10 wt.-% clay-mineral content and 1 for ≤10 wt.-% clay-mineral content. Data highlighted by yellow background were screened out from further interpretation based on criteria given in Section 6.2

Lab ID	Depth [m]	Formation	Physical porosity [%]	Clay min. [wt.-%]	Cl^- (phys. por.) [mg/L_{pw}]	Error [mg/L_{pw}]	Cl^- (clay-min. cont.) [mg/L_{pw}]	Error [mg/L_{pw}]
BEN 1	395.97	Wohlgeschichtete Kalke	3.3	1	5237	3911	4130	1310
BEN 2	407.38	Wohlgeschichtete Kalke	3.9	1	2533	1668	2397	760
BEN 3	417.83	Hornbuck-Schichten	4.2	9	3007	1908	2328	748
BEN 4	428.11	Hornbuck-Schichten	9.5	36	6081	2496	5979	2009
BEN 5	443.83	Effinger Schichten	8.8	13	5134	2179	7643	2472
BEN 6	459.90	Varians-Schichten	11.9	53	6931	2626	6676	2311
BEN 7	467.12	Parkinsoni-Württemb.-Sch.	12.7	51	6494	2416	6894	2378
BEN 8	476.14	Parkinsoni-Württemb.-Sch.	5.8	24	9589	4999	6979	2298
BEN 9	481.11	Parkinsoni-Württemb.-Sch.	13.1	57	7030	2594	7121	2481
BEN 20	482.00	Parkinsoni-Württemb.-Sch.	11.9	42				
BEN 10	489.15	Parkinsoni-Württemb.-Sch.	12.2	52	6977	2623	6988	2416
BEN 11	498.61	Subfurcaten-Schichten	14.3	34	12578	4537	20514	6867
BEN 12	504.45	Subfurcaten-Schichten	12.4	36	9989	3740	13122	4414
BEN 13	507.87	Wedelsandstein-Formation	14.1	50	5861	2121	7094	2445
BEN 21	525.45	Wedelsandstein-Formation	11.7	14				
BEN 14	525.88	Wedelsandstein-Formation	8.1	10	5446	2390	8261	2657
BEN 15	535.49	Wedelsandstein-Formation	9.8	29	6170	2505	7208	2392

Tab. 29: Calculated pore-water concentrations of Cl^- for the Riniken profile

Cl^- (phys. por.) was calculated using porosity obtained from densities; Cl^- (clay-min. cont.) was calculated using porosity derived from clay-mineral content, applying the regression for samples from boreholes Benken and Weiach (Fig. 9). The fraction of anion-accessible porosity was assumed to be 0.5 for rocks with >10 wt.-% clay-mineral content and 1 for ≤10 wt.-% clay-mineral content. Data highlighted by yellow background were screened out from further interpretation based on criteria given in Section 6.2

Lab ID	Depth [m]	Formation	Physical porosity [%]	Clay min. [wt.-%]	Cl^- (phys. por.) [mg/L_{pw}]	Error [mg/L_{pw}]	Cl^- (clay-min. cont.) [mg/L_{pw}]	Error [mg/L_{pw}]
RIN 1	328.34	Murchisonae-Schichten	11.6	40	2993	1144	3420	1157
RIN 2	334.68	Opalinuston	7.6	44	5006	2261	3373	1149
RIN 3	344.72	Opalinuston	10.3	43	3396	1353	3230	1098
RIN 4	352.91	Opalinuston	8.8	59	4015	1698	2517	881
RIN 5	365.03	Opalinuston	11.0	59	2856	1110	2306	807
RIN 6	373.60	Opalinuston	10.0	54	2719	1094	2108	732
RIN 7	385.16	Opalinuston	11.7	57	2360	901	2090	729
RIN 8	395.20	Opalinuston	11.4	65	2563	987	1982	701
RIN 9	406.03	Opalinuston	10.2	50	2931	1169	2468	850
RIN 10	416.28	Opalinuston	10.3	63	3003	1196	2124	749
RIN 11	426.03	Opalinuston	10.5	69	2907	1150	1934	690
RIN 12	436.81	Opalinuston	11.6	71	3075	1174	2264	809
RIN 13	446.51	Opalinuston	10.9	65	2696	1051	1990	704
RIN 14	455.84	Posidonienschiefer	9.7	48	3600	1464	2978	1021
RIN 15	466.07	Obtusus-Ton	10.9	13	2137	834	4117	1331
RIN 16	476.25	Arietenkalk	8.9	39	2862	1208	2479	837
RIN 17	485.67	Insektenmergel	11.3	60	2562	987	2101	737
RIN 18	487.70	Insektenmergel	13.3	66	1634	600	1487	527

Tab. 30: Calculated pore-water concentrations of Cl^- for the Schafisheim profile

Cl^- (phys. por.) was calculated using porosity obtained from densities; Cl^- (clay-min. cont.) was calculated using porosity derived from clay-mineral content, applying the regression for samples from boreholes Benken and Weiach (Fig. 9). The fraction of anion-accessible porosity was assumed to be 0.5 for rocks with >10 wt.-% clay-mineral content and 1 for ≤10 wt.-% clay-mineral content. Data highlighted by yellow background were screened out from further interpretation based on criteria given in Section 6.2

Lab ID	Depth [m]	Formation	Physical porosity [%]	Clay min. [wt.-%]	Cl^- (phys. por.) [mg/L_{pw}]	Error [mg/L_{pw}]	Cl^- (clay-min. cont.) [mg/L_{pw}]	Error [mg/L_{pw}]
SHA 1	963.05	Sowerbyi-Sauzei-Schichten	6.0	27	11754	5978	8388	2777
SHA 2	974.32	Sowerbyi-Sauzei-Schichten	4.5	2	10189	6155	10890	3457
SHA 3	985.03	Sowerbyi-Sauzei-Schichten	7.6	30	8787	3966	7594	2527
SHA 4	994.20	Murchisonae-Schichten	6.7	5	10805	5185	15626	4988
SHA 5	1005.10	Opalinuston	9.6	60	11287	4608	7776	2724
SHA 6	1015.67	Opalinuston	7.4	51	12639	5793	7344	2534
SHA 7	1026.11	Opalinuston	10.1	58	9720	3896	7175	2508
SHA 8	1035.75	Opalinuston	8.1	64	12412	5447	6708	2367
SHA 9	1046.03	Opalinuston	8.2	52	13036	5695	8427	2910
SHA 10	1056.63	Opalinuston	8.0	57	16377	7237	9554	3329
SHA 11	1063.95	Opalinuston	6.3	61	15633	7797	6575	2311
SHA 12	1076.86	Opalinuston	5.8	60	14063	7306	5575	1954
SHA 13	1087.78	Obtusus-Ton	5.3	30	6851	3744	4009	1334
SHA 14	1096.88	Insektenmergel	10.6	68	11431	4500	7864	2797
SHA 15	1105.10	Insektenmergel	10.2	63	9605	3833	6728	2372
SHA 16	1117.57	Schilfsandstein	10.9	53	17442	6811	15184	5253
SHA 17	1127.74	Schilfsandstein	8.6	57	22331	9551	14114	4919
SHA 18	1138.08	Schilfsandstein	4.3	24	29089	18002	15738	5181
SHA 19	1152.15	Gipskeuper	11.4	55	10542	4052	9396	3262
SHA 20	1162.05	Gipskeuper	2.1	10	5892	6240	2113	680
SHA 21	1173.84	Gipskeuper	6.4	14	7759	3837	7977	2584
SHA 22	1184.98	Gipskeuper	9.0	45	15743	6614	12353	4220
SHA 23	1196.99	Gipskeuper	3.3	27	29395	22015	11187	3700
SHA 24	1208.68	Gipskeuper	6.1	27	25170	12673	18316	6064
SHA 25	1218.59	Gipskeuper	1.6	1	1781	2340	667	211
SHA 26	1226.69	Lettenkohle	1.8	0	29099	33894	13238	4192
SHA 27	1234.28	Trigonodus-Dolomit	9.0	4	7303	3065	14936	4760

Tab. 31: Calculated pore-water concentrations of Cl^- for the Weiach profile

Cl^- (phys. por.) was calculated using porosity obtained from densities; Cl^- (clay-min. cont.) was calculated using porosity derived from clay-mineral content, applying the regression for samples from boreholes Benken and Weiach (Fig. 9). The fraction of anion-accessible porosity was assumed to be 0.5 for rocks with >10 wt.-% clay-mineral content and 1 for ≤10 wt.-% clay-mineral content. Data highlighted by yellow background were screened out from further interpretation based on criteria given in Section 6.2

Lab ID	Depth [m]	Formation	Physical porosity [%]	Clay min. [wt.-%]	Cl^- (phys. por.) [mg/L_{pw}]	Error [mg/L_{pw}]	Cl^- (clay-min. cont.) [mg/L_{pw}]	Error [mg/L_{pw}]
WEI 31	271.98	Massenkalk	8.4	16	3031	1308	4048	1315
WEI 32	285.77	Quaderkalk	7.4	24	4466	2050	4225	1391
WEI 33	299.52	Schwarzbach-Schichten	2.8	15	12327	10470	5181	1681
WEI 34	309.33	Schwarzbach-Schichten	9.2	34	5682	2365	5553	1861
WEI 35	320.25	Wangental-Schichten	6.1	14	5582	2827	5526	1789
WEI 36	330.06	Wangental-Schichten	1.7	1	6744	8414	2737	868
WEI 37	330.88	Wangental-Schichten	1.5	4	3594	4905	1163	370
WEI 25	340.51	Küssaburg-Schichten	5.0	11	6419	3626	5557	1792
WEI 38	351.14	Küssaburg-Schichten	1.8	1	5883	6926	2530	802
WEI 39	362.41	Küssaburg-Schichten	3.8	4	3300	2247	2632	839
WEI 40	374.73	Küssaburg-Schichten	5.2	11	6091	3376	5446	1756
WEI 41	386.05	Hornbuck-Schichten	7.9	20	5235	2325	5853	1915
WEI 42	394.91	Effinger Schichten	7.1	17	5016	2345	5366	1747
WEI 43	404.98	Effinger Schichten	6.9	17	4754	2260	4951	1611
WEI 44	415.79	Effinger Schichten	5.7	12	5766	3041	5536	1787
WEI 45	426.14	Effinger Schichten	6.8	21	4679	2239	4307	1412
WEI 46	436.39	Effinger Schichten	9.5	39	5785	2375	5358	1811
WEI 47	450.30	Effinger Schichten	8.6	26	5153	2209	5535	1827
WEI 48	459.69	Effinger Schichten	8.2	21	4890	2131	5605	1836
WEI 49	467.84	Effinger Schichten	6.2	22	6537	3276	5341	1754
WEI 50	476.09	Effinger Schichten	5.9	20	7903	4053	6564	2146
WEI 1	484.14	Varians-Schichten		66			5010	1777
WEI 2	495.46	Württembergica-Schichten		44			5860	1996
WEI 3	506.08	Württembergica-Schichten		49			4687	1612
WEI 4	517.10	Württembergica-Schichten		56			5868	2044
WEI 5	527.86	Parkinsoni-Schichten		39			4070	1375
WEI 6	539.26	Sowerbyi-Sauzei-Schichten		56			5017	1746
WEI 7	549.62	Murchisonae-Schichten		70			4572	1632
WEI 51	560.48	Opalinuston	7.8	17	4296	1915	5065	1650
WEI 8	561.08	Opalinuston		45				
WEI 9	572.80	Opalinuston		63			3620	1276
WEI 52	581.86	Opalinuston	8.1	40	4859	2129	3760	1272
WEI 10	582.04	Opalinuston		61				
WEI 11	594.74	Opalinuston		64			3610	1275
WEI 12	605.34	Opalinuston		66			3582	1269
WEI 13	616.32	Opalinuston		62			3749	1319
WEI 14	627.09	Opalinuston		54			4609	1599
WEI 15	638.09	Opalinuston		68			3761	1337
WEI 16	649.46	Opalinuston		68				
WEI 53	652.20	Opalinuston	10.7	75	5137	2016	3259	1175
WEI 17	660.30	Opalinuston		70			3377	1205
WEI 18	671.89	Posidonienschiefer		38			4934	1664
WEI 19	682.16	Obtusus-Ton		35			6073	2036
WEI 20	693.19	Obtusus-Ton		49			4375	1505
WEI 21	703.88	Insektenmergel		60			6357	2230
WEI 22	715.56	Knollenmergel		45			6913	2359
WEI 54	723.98	Obere Bunte Mergel	13.1	55	5333	1969	5545	1925
WEI 55	736.12	Schilfsandstein	15.5	84	5628	1997	4904	1798
WEI 56	744.63	Gipskeuper	11.8	54	5137	1951	4857	1683
WEI 57	757.94	Gipskeuper	6.6	26	5919	2876	4767	1575
WEI 58	769.10	Gipskeuper	b.d.	10			2752	886
WEI 59	782.38	Gipskeuper	3.1	30	9179	7184	3051	1015
WEI 60	790.71	Gipskeuper	12.5	57	3393	1269	3210	1120
WEI 61	802.29	Gipskeuper	8.0	42	7334	3244	5332	1811
WEI 62	812.25	Gipskeuper	3.4	1	6885	5024	5565	1766
WEI 63	818.50	Lettenkohle	6.8	48	1830	874	1020	350

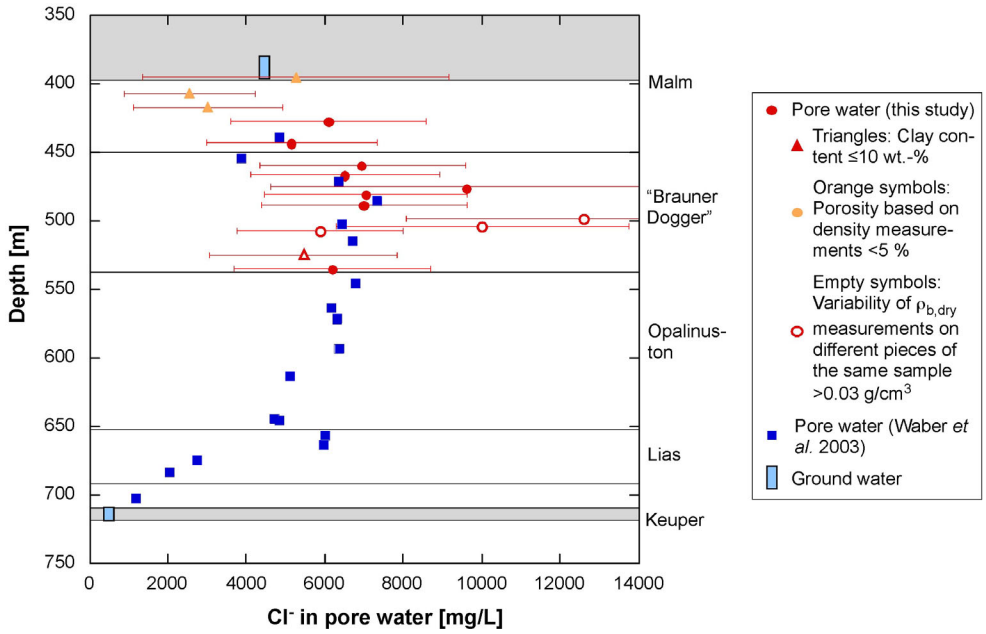

Fig. 13: Cl^- profile for Benken using physical porosity for the recalculation to pore-water concentrations

The fraction of anion-accessible porosity was assumed to be 0.5 for rocks with >10 wt.-% clay-mineral content and 1 for ≤10 wt.-% clay-mineral content. Waber *et al.*'s (2003) data are left as in the original, *i.e.* they refer to water-loss porosity and an anion-accessible porosity fraction of 0.5. Aquifers are shown in grey

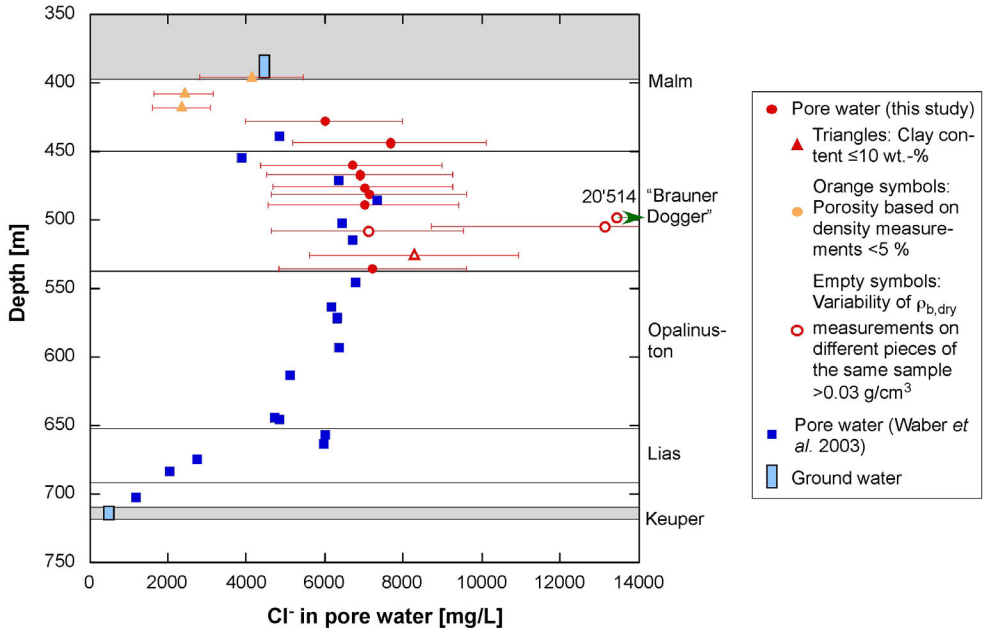

Fig. 14: Cl^- profile for Benken using porosity derived from clay-mineral content for the recalculation to pore-water concentrations

The fraction of anion-accessible porosity was assumed to be 0.5 for rocks with >10 wt.-% clay-mineral content and 1 for ≤10 wt.-% clay-mineral content. Waber *et al.*'s (2003) data are left as in the original, *i.e.* they refer to water-loss porosity and an anion-accessible porosity fraction of 0.5. Aquifers are shown in grey

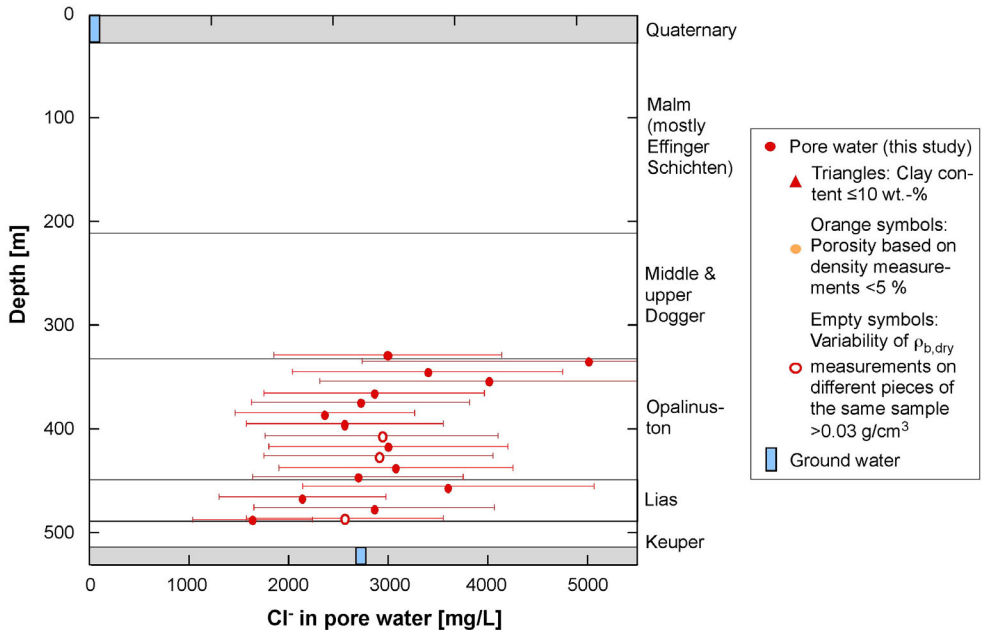

Fig. 15: Cl^- profile for Riniken using physical porosity for the recalculation to pore-water concentrations

The fraction of anion-accessible porosity was assumed to be 0.5 for rocks with >10 wt.-% clay-mineral content and 1 for ≤10 wt.-% clay-mineral content. Aquifers are shown in grey

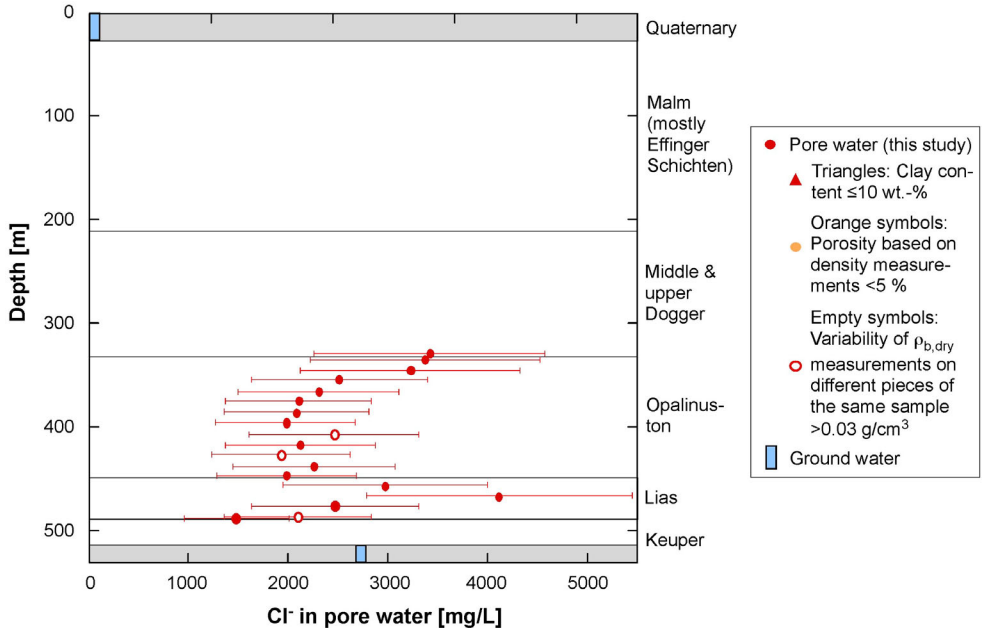

Fig. 16: Cl^- profile for Riniken using porosity derived from clay-mineral content for the recalculation to pore-water concentrations

The fraction of anion-accessible porosity was assumed to be 0.5 for rocks with >10 wt.-% clay-mineral content and 1 for ≤10 wt.-% clay-mineral content. Aquifers are shown in grey

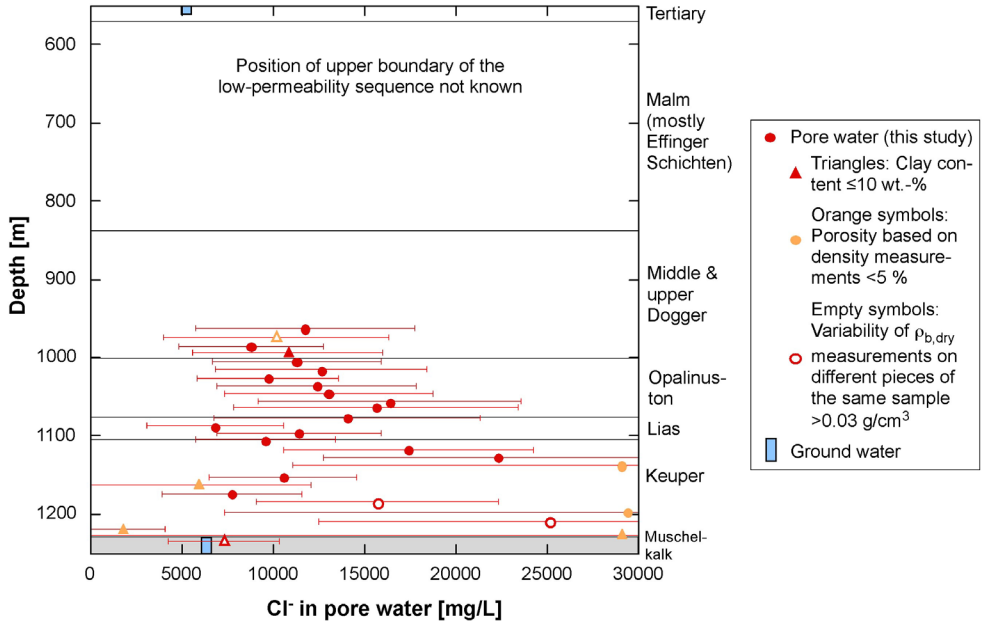

Fig. 17: Cl^- profile for Schafisheim using physical porosity for the recalculation to pore-water concentrations

The fraction of anion-accessible porosity was assumed to be 0.5 for rocks with >10 wt.-% clay-mineral content and 1 for ≤10 wt.-% clay-mineral content. Aquifers are shown in grey

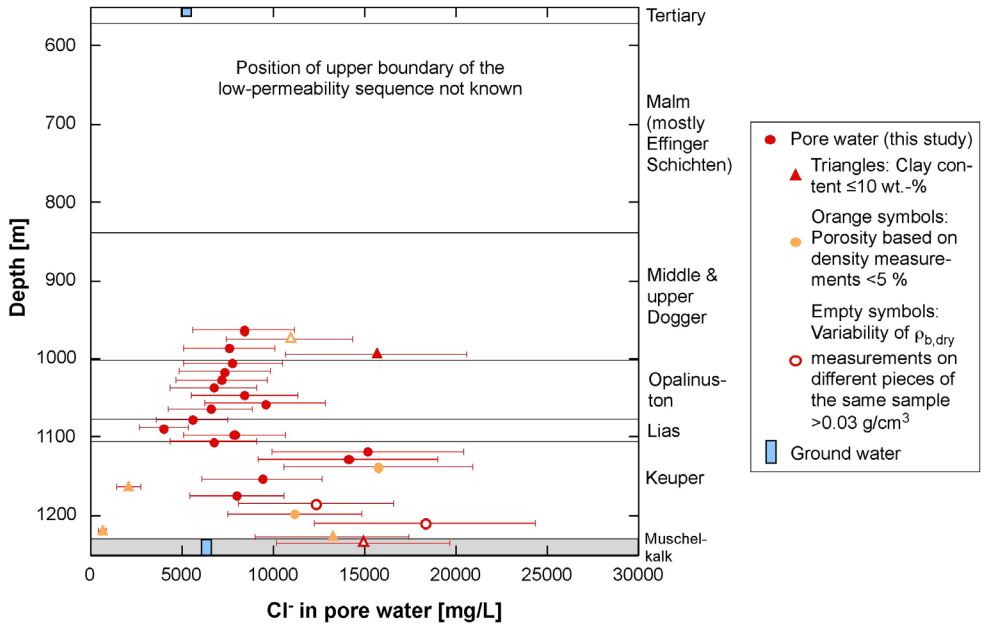

Fig. 18: Cl^- profile for Schafisheim using porosity derived from clay-mineral content for the recalculation to pore-water concentrations

The fraction of anion-accessible porosity was assumed to be 0.5 for rocks with >10 wt.-% clay-mineral content and 1 for ≤10 wt.-% clay-mineral content. Aquifers are shown in grey

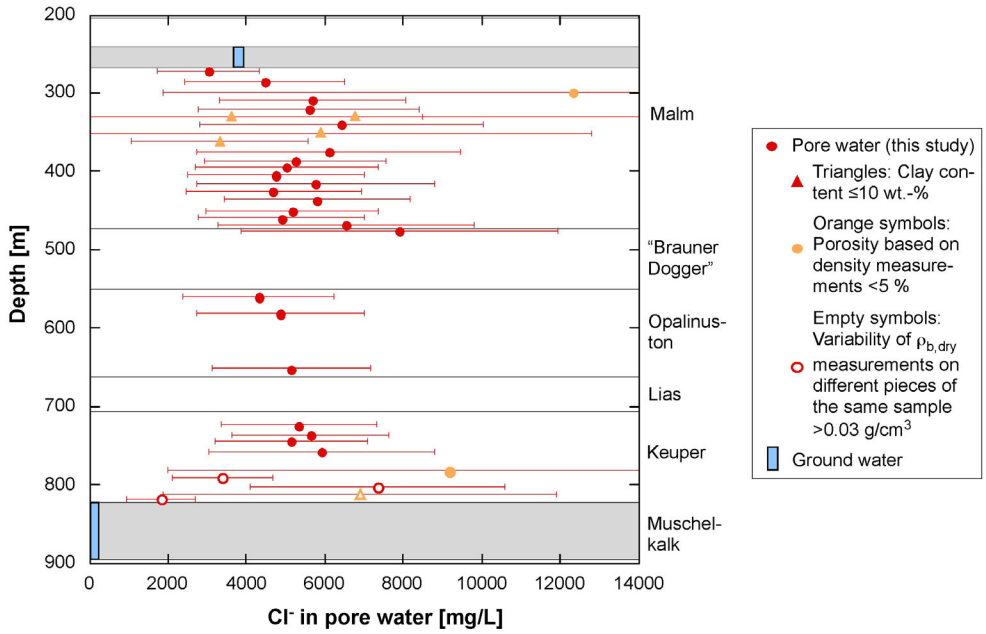

Fig. 19: Cl^- for profile Weiach using physical porosity for the recalculation to pore-water concentrations

The fraction of anion-accessible porosity was assumed to be 0.5 for rocks with >10 wt.-% clay-mineral content and 1 for ≤10 wt.-% clay-mineral content. Aquifers are shown in grey

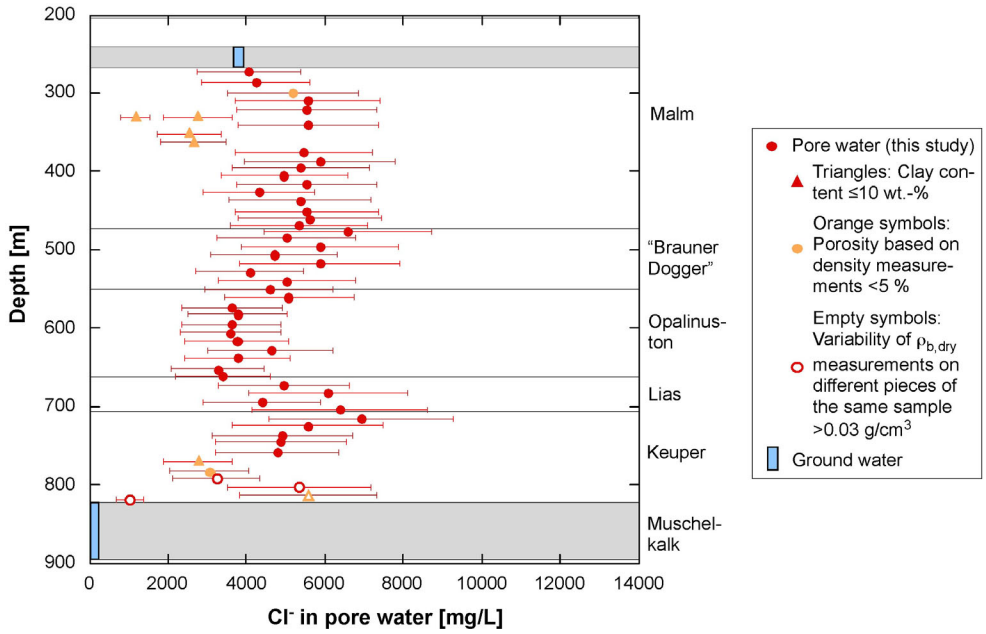

Fig. 20: Cl^- profile for Weiach using porosity derived from clay-mineral content for the recalculation to pore-water concentrations

The fraction of anion-accessible porosity was assumed to be 0.5 for rocks with >10 wt.-% clay-mineral content and 1 for ≤10 wt.-% clay-mineral content. Aquifers are shown in grey

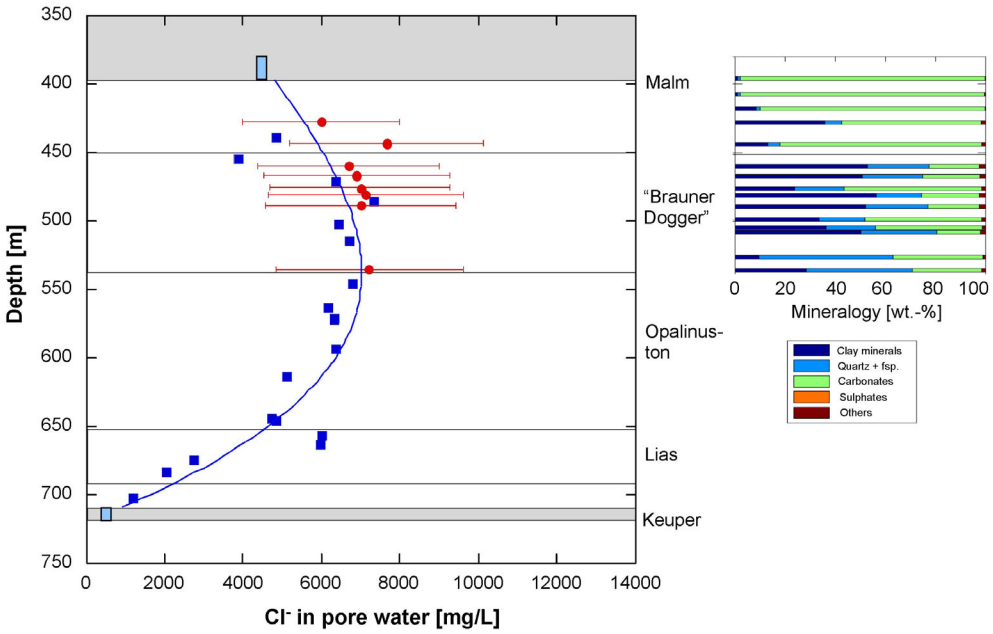

Fig. 21: Screened Cl^- profile for Benken using porosity derived from clay-mineral content for the recalculation to pore-water concentrations

The fraction of anion-accessible porosity was assumed to be 0.5 for rocks with >10 wt.-% clay-mineral content and 1 for ≤10 wt.-% clay-mineral content. Only the screened data set is shown, together with a polynomial fit. Waber *et al.*'s (2003) data (blue squares) are left as in the original, *i.e.* they refer to water-loss porosity and an anion-accessible porosity fraction of 0.5

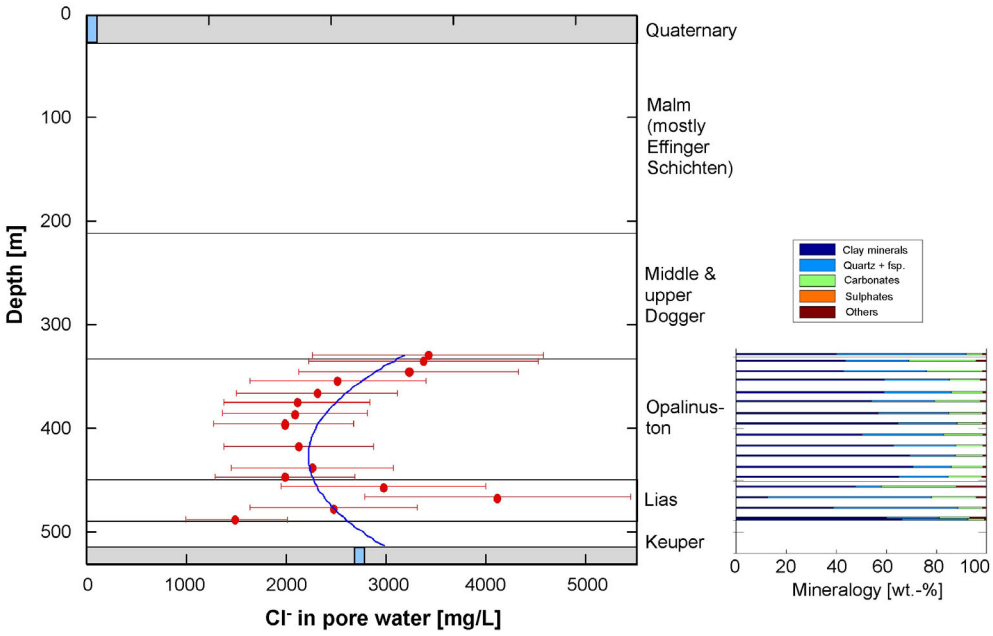

Fig. 22: Screened Cl^- profile for Riniken using porosity derived from clay-mineral content for the recalculation to pore-water concentrations

The fraction of anion-accessible porosity was assumed to be 0.5 for rocks with >10 wt.-% clay-mineral content and 1 for ≤10 wt.-% clay-mineral content. Only the screened data set is shown, together with a polynomial fit

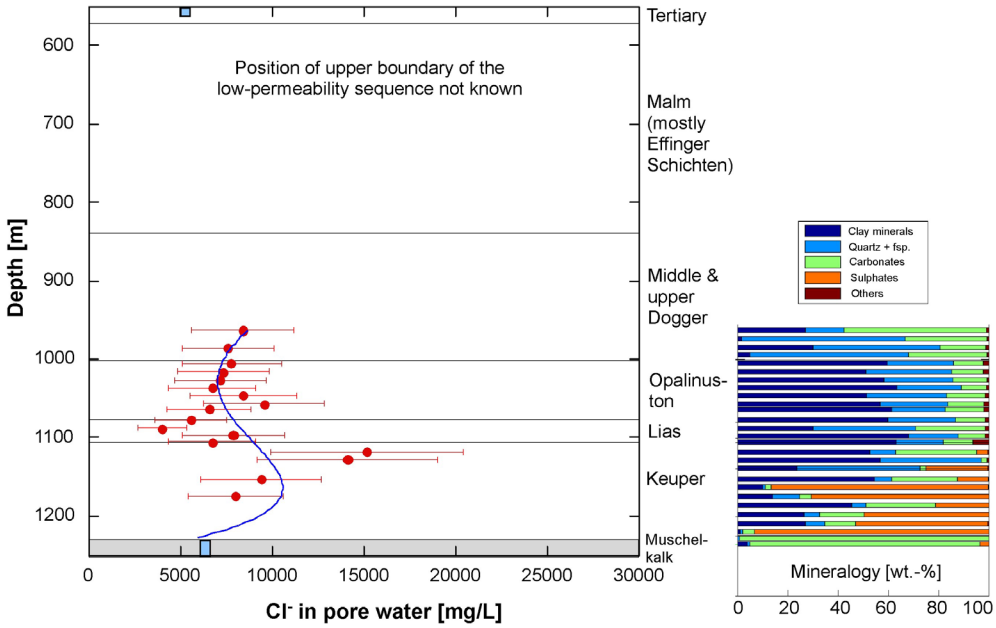

Fig. 23: Screened Cl^- profile for Schafisheim using porosity derived from clay-mineral content for the recalculation to pore-water concentrations

The fraction of anion-accessible porosity was assumed to be 0.5 for rocks with >10 wt.-% clay-mineral content and 1 for ≤10 wt.-% clay-mineral content. Only the screened data set is shown, together with a polynomial fit

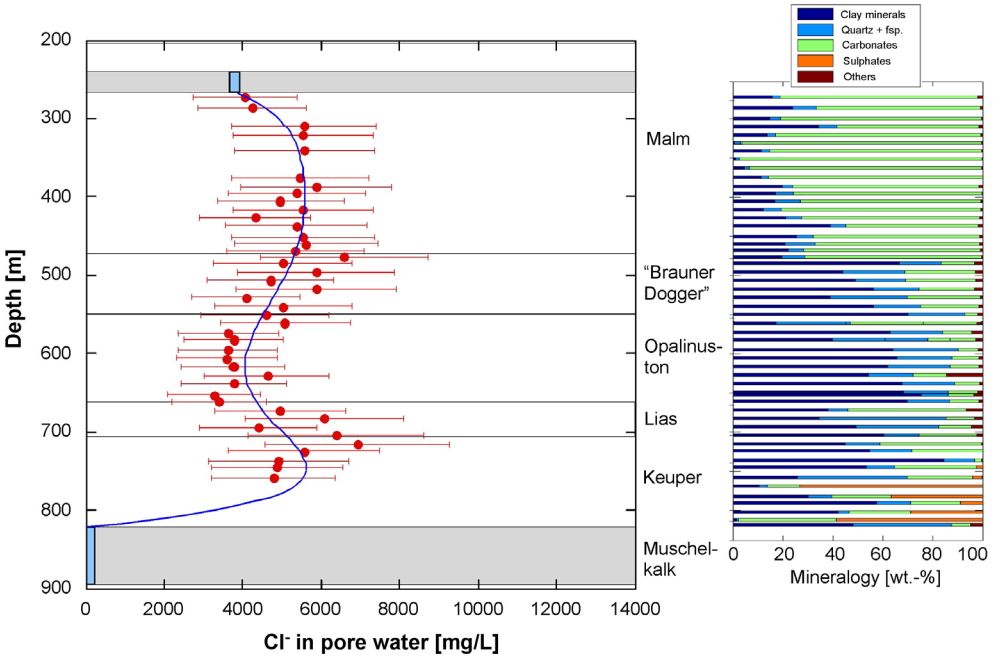

Fig. 24: Screened Cl^- profile for Weiach using porosity derived from clay-mineral content for the recalculation to pore-water concentrations

The fraction of anion-accessible porosity was assumed to be 0.5 for rocks with >10 wt.-% clay-mineral content and 1 for ≤10 wt.-% clay-mineral content. Only the screened data set is shown, together with a polynomial fit

7 References

Bruland, K.W. & Lohan, M.C. 2003. Controls of trace metals in seawater. In: H.D. Holland & K.K. Turekian (eds) Treatise on Geochemistry, vol. 6 (The oceans and marine geochemistry), 23-47

Füchtbauer, H., 1988. Sedimente und Sedimentgesteine. Schweizerbart Verlagsbuchhandlung, Stuttgart, Germany

Gimmi, T. & Waber, H.N. 2004. Modelling of tracer profiles in pore water of argillaceous rocks in the Benken borehole: Stable water isotopes, chloride and chlorine isotopes. Nagra Tech. Rep. NTB 04-05

Gimmi, T., Waber, H.N., Gautschi, A. & Rübel, A. 2007. Stable water isotopes in pore water of Jurassic argillaceous rocks as tracers for solute transport over large spatial and temporal scales. Water Resources Research 43, W04410

Koroleva, M., Alt-Epping, P. & Mazurek, M. 2011. Large-scale tracer profiles in a deep claystone formation (Opalinus Clay at Mont Russelin, Switzerland): implications for solute transport processes and transport properties of the rock. Chemical Geology 280, 284-296

Mäder, U. 2009a. Reference pore water for the Opalinus Clay and "Brown Dogger" for the provisional safety-analysis in the framework of the sectoral plan - interim results (SGT-ZE). Nagra Arbeitsber.

Mäder, U. 2009b. Reference pore water for the Effingen Member (Standortregion Südjura) for the provisional safety-analysis in the framework of the sectoral plan - interim results (SGT-ZE). Nagra Arbeitsber.

Matter, A., Peters, T., Isenschmid, C., Bläsi, H.R. & Ziegler, H.J. 1987. Sondierbohrung Riniken – Geologie. Nagra Tech. Ber. NTB 86-02

Matter, A., Peters, T., Bläsi, H.R., Meyer, J., Ischi, H. & Meyer, C. 1988a. Sondierbohrung Weiach – Geologie. Nagra Tech. Ber. NTB 86-01

Matter, A., Peters, T., Bläsi, H.R., Weiss, H.P. & Schenker, F. 1988b. Sondierbohrung Schafisheim – Geologie. Nagra Tech. Ber. NTB 86-03

Mazurek, M. 2011. Aufbau und Auswertung der Gesteinsparameter-Datenbank für Opalinuston, den "Braunen Dogger", Effinger Schichten und Mergel-Formationen des Helvetikums. Nagra Arbeitsber.

Mazurek, M., Hurford, A. J. & Leu, W. 2006. Unravelling the multi-stage burial history of the Swiss Molasse Basin: Integration of apatite fission track, vitrinite reflectance and biomarker isomerisation analysis. Basin Research 18, 27-50

Mazurek, M., Alt-Epping, P., Bath, A., Gimmi, T. & Waber, H. N. 2009. Natural tracer profiles across argillaceous formations: The CLAYTRAC project. OECD/NEA report 6253, OECD Nuclear Energy Agency, Paris, France

Mazurek, M., Meier, D. & Müller, H. 2010. WS-H experiment: Geological, petrophysical and geochemical characterisation of drillcores from borehole BHG-B11. Mont Terri Technical Note TN 2010-22, Mont Terri Consortium, St. Ursanne, Switzerland

Mazurek, M., Alt-Epping, P., Bath, A., Gimmi, T., Waber, H. N., Buschaert, S., De Cannière, P., De Craen, M., Gautschi, A., Savoye, S., Vinsot, A., Wemaere, I. & Wouters, L. 2011. Natural tracer profiles across argillaceous formations. Applied Geochemistry 26, 1035-1064

Nagra 1988. Sondierbohrungen Böttstein, Weiach, Riniken, Schafisheim, Kaisten Leuggern: Fluid Logging - Temperatur-. Leitfähigkeits- und Spinner-Flowmeter-Messungen. Nagra Tech. Ber. NTB 85-10

Nagra 1989. Sondierbohrung Weiach: Untersuchungsbericht. Nagra Techn. Ber. NTB 88-08

Nagra 1990. Sondierbohrung Riniken: Untersuchungsbericht. Nagra Tech. Ber. NTB 88-09

Nagra 1992. Sondierbohrung Schafisheim: Untersuchungsbericht. Nagra Tech. Ber. NTB 88-11

Nagra 2001. Sondierbohrung Benken: Untersuchungsbericht. Nagra Tech. Ber. NTB 00-01

Nagra 2002. Projekt Opalinuston - Synthese der geowissenschaftlichen Untersuchungsergebnisse. Nagra Tech. Ber. NTB 02-03

Nagra 2008. Vorschlag geologischer Standortgebiete für das SMA- und das HAA-Lager – Geologische Grundlagen. Nagra Tech. Ber. NTB 08-04

Pearson, F.J., Arcos, D., Bath, A., Boisson, J.Y., Fernandez, A.M., Gaebler, H.E., Gaucher, E., Gautschi, A., Griffault, L., Hernan, P., and Waber, H.N. 2003. Geochemistry of water in the Opalinus Clay formation at the Mont Terri Rock Laboratory - Synthesis Report. Swiss Federal Office for Water and Geology (FOWG), Bern, Switzerland, Geology Series, Nr. 5

Waber, H.N., Pearson, F.J., Hobbs, M.Y. & Oyama, T. 2003. Sondierbohrung Benken: Characterisation of pore water from argillaceous rocks. Nagra Intern. Ber.